Bull Volcanol (2017) 79: 3
DOI 10.1007/s00445-016-1085-5

RESEARCH ARTICLE

New insights into Holocene eruption episodes from proximal deposit sequences at Mt. Taranaki (Egmont), New Zealand

Rafael Torres-Orozco[1] · **Shane J. Cronin**[1,2] · **Natalia Pardo**[3] · **Alan S. Palmer**[1]

Received: 12 July 2016 / Accepted: 17 November 2016 / Published online: 19 December 2016

Abstract Upper stratovolcano flanks contain the most nuanced depositional record of long eruption episodes, but steep, irregular terrain makes these sequences difficult to correlate and interpret. This necessitates development of a detailed and systematic approach to describing localized depositional facies and relating these to eruptive processes. In this work, the late-Holocene eruption history of Mt. Taranaki/Egmont, New Zealand, was re-assessed based on a study of proximal deposits spanning the ^{14}C-dated age range of ~5.0–0.3 cal ka B.P. Mt. Taranaki is a textbook-example stratovolcano, with geological evidence pointing to sudden switches in scale, type and frequency of eruptions over its ~130 ka history. The proximal stratigraphy presented here almost doubles the number of eruptions recognized from previous soil-stratigraphy studies. A total of 53 lithostratigraphic bed-sets record eruptions of the summit crater and parasitic vents like Fanthams Peak (the latter between ~3.0 and 1.5 cal ka B.P.). At least 12 of the eruptions represented by these bed-sets comprise deposits comparable with or thicker than those of the latest sub-Plinian eruption of AD 1655. The largest eruption episode represented is the 4.6–4.7-cal ka B.P. Kokowai. Contrasting eruption styles were identified, from stable basaltic-andesite eruption columns at Fanthams Peak, to andesitic lava-dome extrusion, blasts and partial collapse of unstable eruption columns at Mt. Taranaki's summit. The centemetre-scale proximal deposit descriptions were used to identify several previously unknown, smaller eruption events. These details are indispensable for building a comprehensive probabilistic event record and in the development of realistic eruptive scenarios for complex eruption episodes prior to re-awakening of a volcano.

Keywords Andesitic volcanoes · Explosive volcanism · Proximal lithostratigraphy · Eruption history · Volcanic hazards

Editorial responsibility: L. Capra

✉ Rafael Torres-Orozco
r.torres-orozco@massey.ac.nz

[1] Volcanic Risk Solutions, Massey University, Private Bag, Palmerston North 11 222, New Zealand

[2] School of Environment, University of Auckland, Private Bag, Auckland 92 019, New Zealand

[3] Department of Geoscience, University of los Andes, Cr 1 #18A, -12 Bogotá, Colombia

Introduction

Andesitic stratovolcanoes have generated some of the most disruptive and deadliest Plinian and sub-Plinian historical eruptions (e.g. Bourdier et al. 1997; Coltelli et al. 1998; Cioni et al. 2000; Carn et al. 2009; Saucedo et al. 2010; Surono et al. 2012; Cronin et al. 2013). Ongoing population growth on the fertile ring plains and debris fans surrounding active volcanoes constantly exacerbates vulnerability to volcanic activity (e.g. Alberico et al. 2011; Cronin et al. 2013). Within increasing populations at risk, there is a need to develop the most comprehensive eruptive frameworks possible prior to re-awakening of andesitic volcanoes, in order to develop high-precision hazard assessments and scenarios that encompass diverse paths of progression that an eruption sequence might follow.

In many past studies, eruption histories have been inferred from investigations of medial and distal deposits in locations where undisturbed deposits in low-relief depositional environments allow accurate sedimentological determinations (e.g. Pardo et al. 2012a, b) and regional tephrostratigraphic

reconstructions (e.g. Neall 1972; Alloway et al. 1995; Andreastuti et al. 2000). There are, however, limitations of medial-distal volcanic records, particularly in humid tropical or temperate environments where rapid weathering and soil formation, along with vegetation, obscures and modifies primary deposits, hindering detailed volcanological interpretation (e.g. Alloway et al. 1995; Espindola et al. 2010; Saucedo et al. 2010; Avellan et al. 2014). Moreover, the medial pyroclastic/volcaniclastic data sets could be biased towards events that produce widely dispersed fallouts, i.e. mainly large-volume and highly explosive events. Also, medial deposits usually provide little detail of the progression of any eruption (i.e. opening, pre-, syn- and post-climactic phases), and they certainly do not represent all eruptions (e.g. lavas do not reach the medial environment). For this reason, it is often difficult to develop detailed eruption scenarios, of a clear understanding of the physical processes involved (cf. Houghton et al. 2004; Platz et al. 2007; Cioni et al. 2008).

Proximal pyroclastic sequences, while challenging to access, may contain a more complete and less-modified record of eruptive episodes than do more-distal sites. Their main limitation is that they normally preserve only the youngest part of the geological record due to remobilization and burying of older deposits by, e.g. repeated cone collapse and lava flow deposition, in addition to other erosive processes (e.g. fluvial, mass-movement and eolian). Despite this, many interfluve and ridge areas contain well-preserved deposit sequences that may represent most, or even all, of the phases of an ancient eruption (e.g. Macias et al. 1997; Houghton et al. 2004; Arce et al. 2003, 2005; Platz et al. 2007, 2012; Cronin et al. 2013; Avellan et al. 2014; Kim et al. 2014) and consequently may provide the foundation for understanding the potential pre-eruptive, opening, syn- and post-eruptive phases of a future eruption episode (e.g. Cioni et al. 2008).

The andesitic stratovolcano Mt. Taranaki (in the western part of the North Island of New Zealand) has produced several large, explosive eruptions and frequent mildly explosive activity since 5 ka, as seen primarily from ring-plain records and studies of isolated deposits from single events in proximal sites (Alloway et al. 1995; Platz et al. 2007; Turner et al. 2008a, b). Past studies of ring-plain deposits included lapilli fall beds contained within soils, together with interbedded debris-flow and debris-avalanche deposits (e.g. Zernack et al. 2009, 2011). These were used to set up a Tephra Formation-based stratigraphic framework (Neall 1972; Alloway et al. 1995), and an understanding of major periods of cone growth and cone collapse. Apart from good information about fall-deposit distribution, the available stratigraphic data lack the detail needed for precise volcanological assessment, and many of the lateral correlations are tentative because they are based primarily on stratigraphic proximity and similar lapilli features (colour, grain size, shape etc.). A parallel set of studies has focussed on the radiocarbon dating of volcanic deposits (mainly fall deposits) in swamp and lake sediments. This provided the event data for forecasting eruption frequencies and magmatic evolution paths, suggesting a probability of 0.52 for an eruption over the next 50 years from Mt. Taranaki (Turner et al. 2008a, 2009, 2011a).

In this work, we aim to refine and expand knowledge of the late-Holocene eruption history of Mt. Taranaki/Egmont, New Zealand, based on detailed analysis of proximal pyroclastic sequences, particularly concentrating on bed, contact and sedimentological features (cf. Arce et al. 2003, 2005; Cronin et al. 2013; Kim et al. 2014). We use these data to fill the gaps between the distal lake- and swamp-core deposits and the sparse tephras within medial soils, and to build a strong geological framework for understanding the opening and closing phases of typical explosive andesitic eruptions. The complex suite of deposits necessitated development of a hierarchical framework for description of the deposits and of the parental eruptions and processes that generated them. This approach can be broadly applied to any pyroclastic sequence but is especially valuable in proximal deposit sequences where a wide variety of deposits may represent emplacement periods from seconds to a few years.

Geological setting and previous work

The North Island of New Zealand lies along the convergent boundary between the Australian and Pacific Plates, with the latter being subducted along the Hikurangi Trough (HT; Henrys et al. 2003; Fig. 1). This subduction system is associated not only with the NNE-SSE-aligned Taupo Volcanic Zone (TVZ; Wilson et al. 1995), located ~280 km to the west of the HT and dominated by rhyolitic volcanoes in the central portion (Fig. 1) but also with the andesitic volcanism produced at the northern and southern extremities of the TVZ (e.g. Mt. Ruapehu) and with the most westerly andesitic volcanism in the North Island (e.g. Mt. Taranaki; Price et al. 2005; Fig. 1).

About 400 km to the west of the HT, 130 km from the TVZ, lies the Quaternary and NNW-SSE trending Taranaki Volcanic Lineament (TVL; Neall 1979; Fig. 1) over the eastern side of the mid-Cretaceous to present-day extensional and NE-SW trending Cape Egmont Fault Zone (King and Thrasher 1996). The TVL is made up of four high-K hornblende-rich andesitic volcanoes, <1750 ka B.P. and younging to the south (i.e. Paritutu, Kaitake, Pouakai and Mt. Taranaki; Price et al. 2005 Fig. 1), which contrast in mineralogy with the two-pyroxene andesitic products being produced concurrently in the southern TVZ. Volcanic products of the TVL cover the entire ~1500 km^2 Taranaki Peninsula and cap mid-Paleozoic to mid-Cretaceous plutonic rocks of the Median Tectonic Zone (Mortimer et al. 1997) and a 6–9-km-thick early to

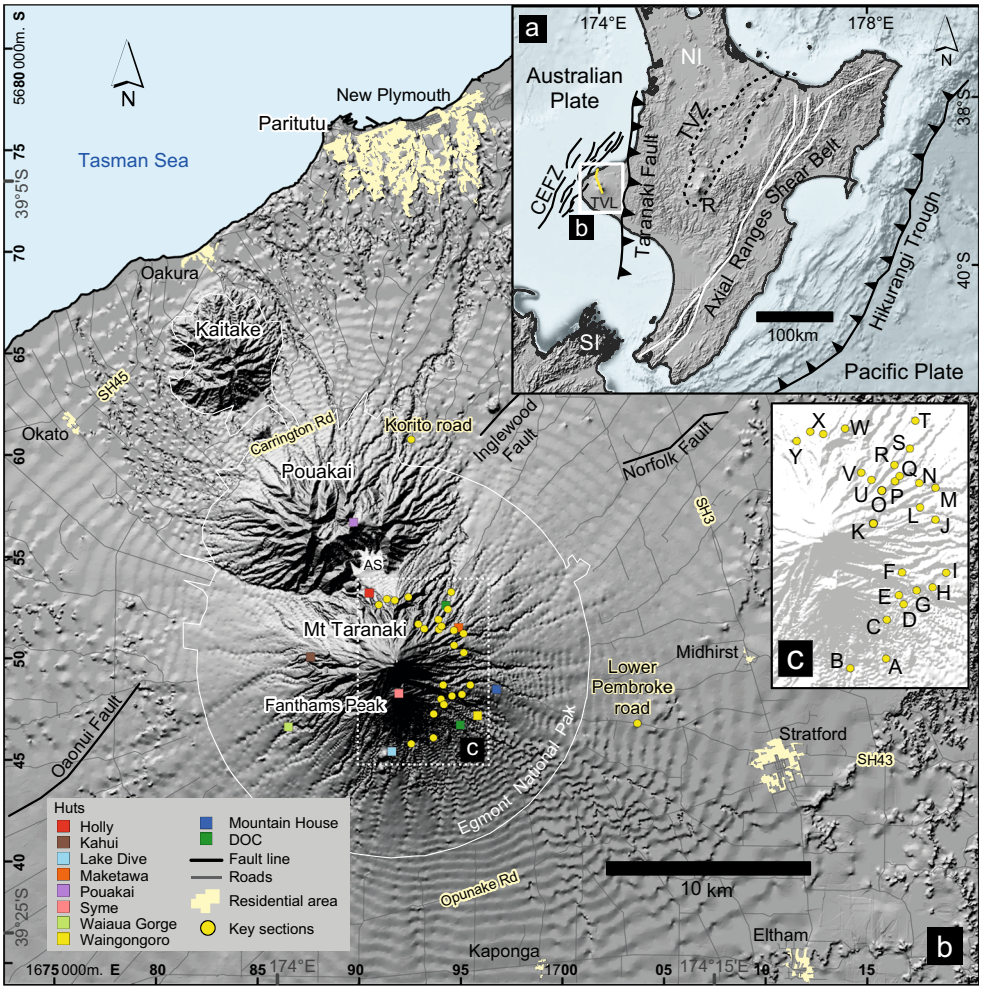

Fig. 1 **a** Tectonic setting of the North Island (*NI*) of New Zealand (modified from King and Thrasher 1996; Henrys et al. 2003; Price et al. 2005; Platz et al. 2007). *CEFZ* Cape Egmont Fault Zone, *R* Mount Ruapehu, *SI* South Island, *TVL* Taranaki Volcanic Lineament (*yellow line*), *TVZ* Taupo Volcanic Zone. **b** Zoomed area of the Taranaki Volcanic Lineament (Neall 1979), which comprises four Pleistocene-Holocene, southwards-younging andesitic volcanoes or their eroded volcanic edifice remnants: Paritutu, Kaitake, Pouakai and Mt. Taranaki (along with the parasitic cone of Fanthams Peak). *AS* Ahukawakawa swamp, *DOC* Department of Conservation Visitor Centre, *SH* principal state highways and other roads connecting residential areas. **c** Zoomed area of the proximal eastern flanks of Mt. Taranaki and the studied key sections. Coordinate system: NZGD 2000 New Zealand Transverse Mercator

mid-Cretaceous sequence of oil- and gas-rich sediments of the Taranaki Basin (King and Thrasher 1996).

Mt. Taranaki/Egmont is the youngest volcano in the extreme south of the TVL with a known eruption record spanning ~130 ka B.P. to AD 1800 (Alloway et al. 2005; Zernack et al. 2011; Platz et al. 2012; Fig. 1). It comprises a 2518-m-high upper cone with a basal area of 25 km^2 and ~12 km^3 in volume, surrounded by a 1000-km^2 ring plain of volcaniclastic debris, which is up to 150 km^3 in volume (Neall et al. 1986; Zernack et al. 2011). The edifice above ~1400 m is considerably younger than the ring plain, with past cones having been repeatedly destroyed by at least 12 massive debris avalanches since ~130 ka. The latest, and one of the smallest, collapses was at ~7.5 ka B.P. (i.e. Opua Formation; Neall 1979; Zernack et al. 2011). On the volcano, lava flows of the ~8-ka B.P. Warwicks Castle Group (Neall 1979; Stewart et al. 1996) constitute the core of the present-day volcanic edifice. The western side of the crater rim likely collapsed in a series of eruptions over the last 800 years (Procter et al. 2010), and remnants of the AD 1800 Sisters dome make up the present summit inside the crater (Platz et al. 2012). The symmetry of the volcano is broken in the southeast by the 1962-m-high basaltic and basalt-andesitic parasitic cone of Fanthams Peak (Stewart et al. 1996; Fig. 1). Due to the splitting of the Opua Debris-avalanche deposit, Fanthams Peak is postulated to have existed before 7 ka B.P. (Neall 1979), but only eruptions since ~3.3 ka B.P., continuing until ~1.8 ka B.P. from this vent have been confirmed (Whitehead 1976; Turner et al. 2008b).

The volcanic history of Mt. Taranaki is characterized by cycles of cone growth to a critical height/size, followed by a catastrophic edifice collapse (Neall et al. 1986; Zernack et al. 2009, 2011). Cone growth includes effusive, lava and dome-forming volcanism, intercalated with periods of highly explosive, Plinian to sub-Plinian eruptions on average 300–500-year intervals, and smaller, strombolian or vulcanian-style eruptions on intervals of ~50–80 years (Alloway et al. 1995; Platz et al. 2007; Turner et al. 2011a). Many of the pyroclastic fall deposits over the last ~30 ka B.P. were mapped northeast and southeast of the volcano within 20 'Tephra Formations' (Neall 1972; Alloway et al. 1995, 2005). Some of the largest known explosive eruptions in Mt. Taranaki's history are recorded by fall deposits dated to within the last 5 ka B.P. and distributed generally east of the volcano, including: the ~5–4.5-ka B.P. Tariki, ~4.1-ka B.P. Korito, ~3.6-ka B.P. Inglewood and ~3.3–2.9-ka B.P. Manganui tephras (Whitehead 1976; Alloway et al. 1995). Some of the youngest fall deposits, e.g. the ~1.5–1.3-ka B.P. Kaupokonui Tephra (Neall and Jansen 1984), were deposited concurrently with ~1.6–1.3 ka B.P. lava flows (Stewart et al. 1996; Neall 2003). In addition to such explosive vents, lava domes also erupted on the northern and southern volcano flanks during the last ~7 ka (Neall et al. 1986; Platz et al. 2012).

The most recent volcanism includes the 0.8–0.4-ka B.P. summit lavas (Downey et al. 1994) that shape most of the present-day upper cone and, at least, six dome-growth and collapse phases recorded by block-and-ash flows (BAFs) and related surge units. These PDC deposits are exposed in proximal areas, mostly on the western flanks (Platz et al. 2012), associated with the Newall, Waiweranui and Puniho ash deposits (Druce 1966; Neall 1972).

The most recent sub-Plinian eruption produced the AD 1655 Burrell Lapilli (Druce 1966; Neall 1972; Topping, 1971), 3×10^6 m^3 of pyroclastic density current deposits and 3.2×10^8 m^3 of fall deposits from a ~14-km-high eruption column (Platz et al. 2007). It was followed by AD 1800–1755 effusive and small explosive events producing the Tahurangi Ash (Druce 1966; Neall 1972), then finally the Sisters dome (Platz et al. 2012).

Methodology

Field methodology

Twenty-five proximal exposures (~900–1350-m-high) were studied around Mt. Taranaki, inside the Egmont National Park and within ~1–4 km of the summit (Figs. 1 and 2). Some of these sections were examined by Turner et al. (2008b, 2011a). On the central eastern flanks of Mt. Taranaki, 3–8-m-thick pyroclastic deposits generally cap flat-topped ridges and interfluves between >100-m-deep, steep-sided valleys. The pumice-dominated deposits generally overlie 12–20-m-thick stacks of coarse lithic-rich breccias and volcaniclastic sands and gravels. On the southern, southeastern and northern volcano flanks, the uppermost pyroclastic deposits expand to 12–15 m thickness and cap thinner massive ash deposits, along with ubiquitous volcaniclastic gravelly sands. These uppermost pyroclastic deposits preserve an eruptive record of up to ~10 ka B.P. (Turner et al. 2011a); however, at the majority of sites, <5 ka B.P. deposits are best preserved. By contrast, the western flanks are covered by thick post-AD 1000 lithic breccias interpreted as BAFs and associated downslope lahar deposits (Platz et al. 2012), which overlie a thick paleosol formed within a sequence of deeply weathered medial ash (Neall 1972).

Some distinctive fall deposits are useful marker horizons in the studied stratigraphic profiles, defined earlier as the Maketawa and Kaupokonui Tephra Formations (Whitehead 1976; Franks 1984; Fig. 2). Medial ring-plain deposits and distal lake sediment profiles (Neall 1972; Alloway et al. 1995, Turner et al. 2008a, 2009) were used to aid overall correlation; however, the proximal stratigraphy is much more intricate, such that close hand-over-hand mapping was needed to reconstruct complex pyroclastic lithofacies architecture.

At each flank exposure, field sedimentary logs were recorded, including data of bed thickness, geometry, contacts, sedimentary structures, sorting (using 1st-order field sorting classes of Cas et al. 2008), framework, grain size (using terminology of White and Houghton 2006), grading and syn-depositional deformational structures, clast texture (e.g. colour, shape, crystallinity and vesicularity), and lithology/componentry (vesicular and dense-lithic juveniles and altered or accidental lithics), following schemes applied in similar types of deposits (e.g. Macias et al. 1997; Arce et al. 2003, 2005; Cioni et al. 2000, 2008; Cronin et al. 2013; Kim et al. 2014). Detailed descriptions were combined into a composite stratigraphic column (Fig. 3) which approximates a theoretical maximum thickness for the whole pyroclastic, epiclastic (i.e. sediments produced from syn- and post-eruptive remobilization-erosion, resedimentation and/or reworking-of pyroclastic deposits; Cas et al. 2008) and soil deposits studied, combining field thicknesses of the most representative exposures.

Mapping criteria

Deposits mappable at 1:25,000 scale with clear recognizable lithology, lithofacies variations and basal-and-capping boundaries were formally classified into *Formations*, subdivided in *Members*, according to the rules of the International Stratigraphic Guide (Salvador 1994). Member is the formal name for a *bed-set* within a defined Formation. However, in most cases, the criteria for defining Formations was not achieved, and deposits were only referred as individual bed-sets constituted by

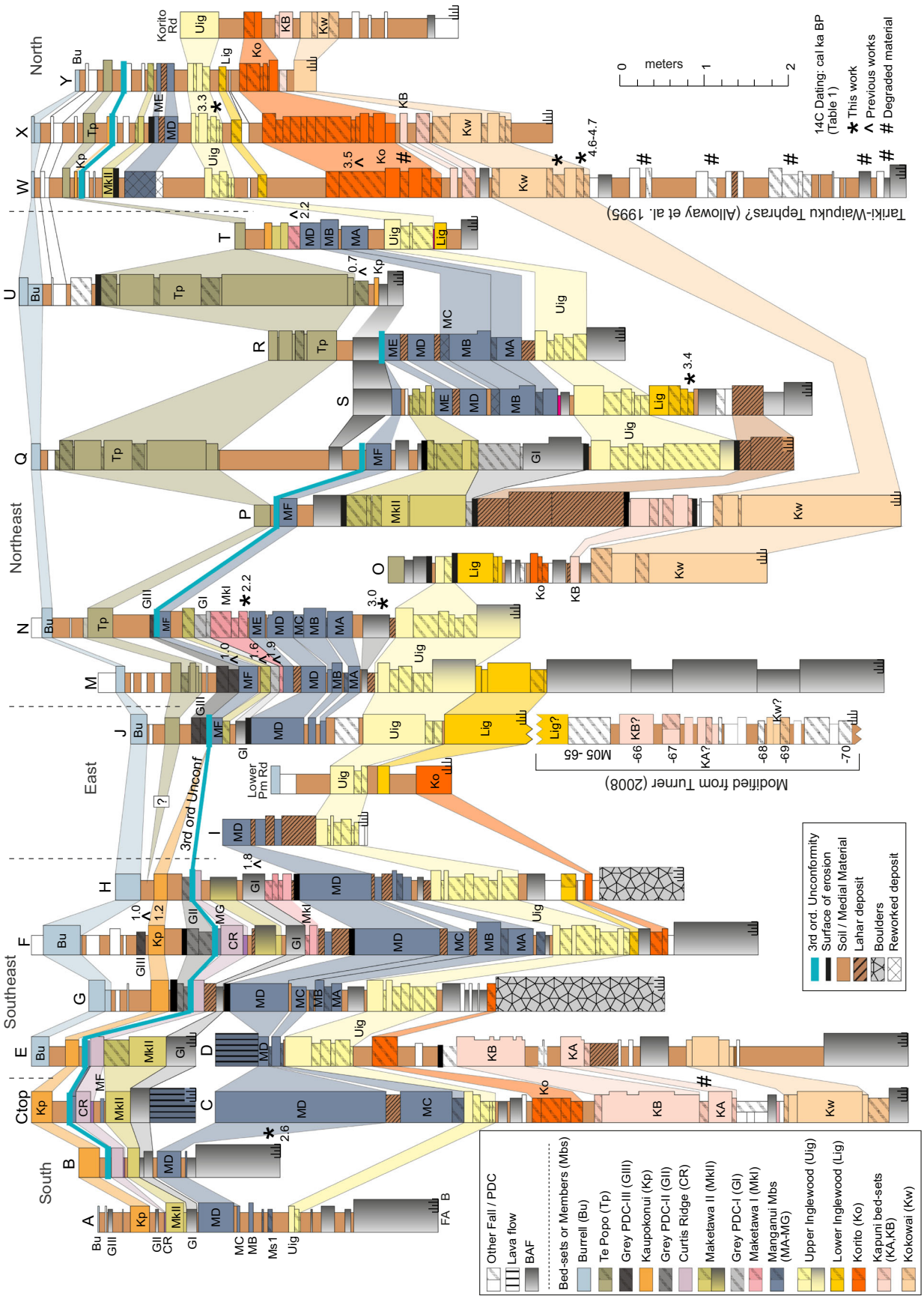

Fig. 2 Stratigraphic correlation of the late-Holocene pyroclastic sequence studied in proximal sections on the eastern flanks of Mt. Taranaki

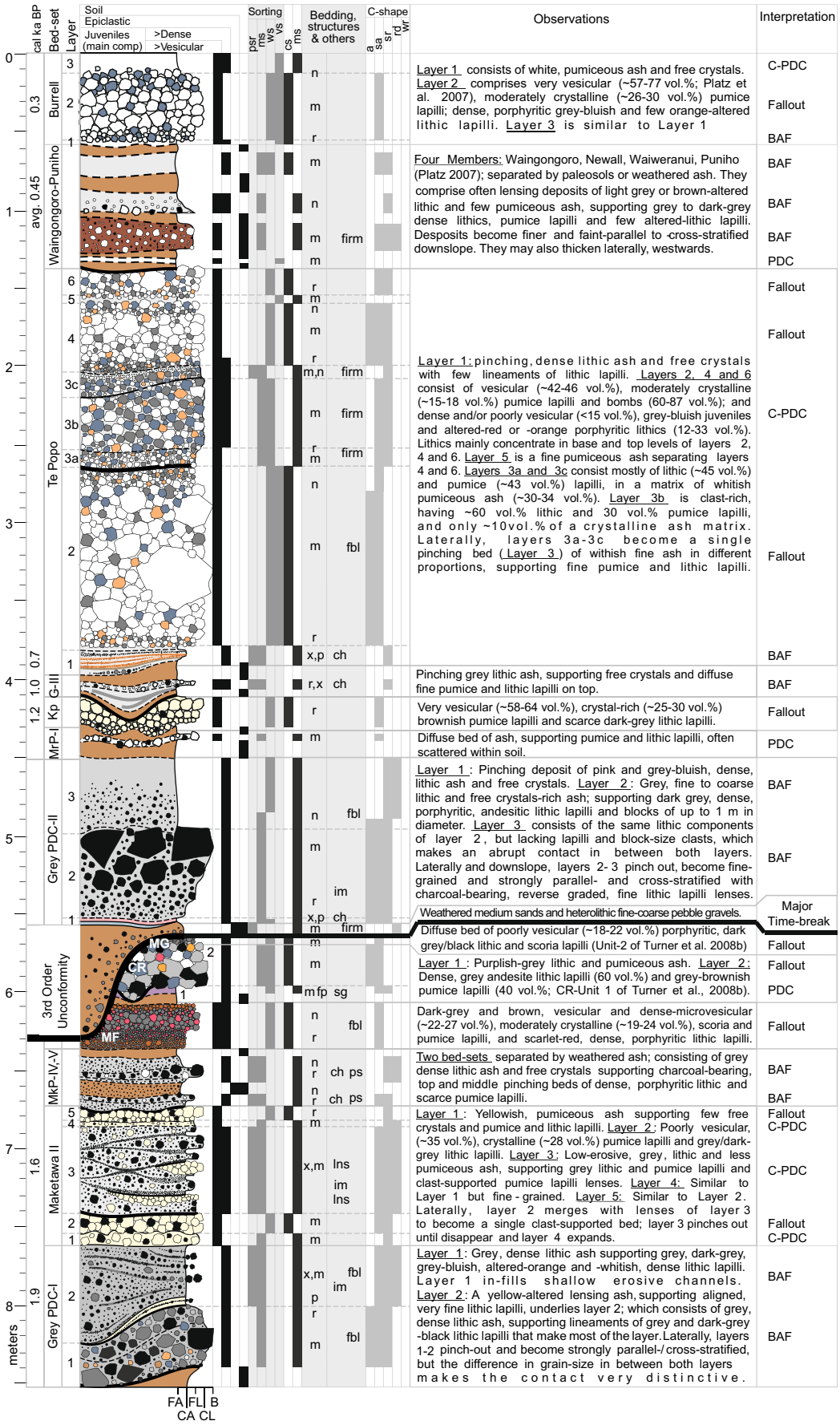
cal ka BP
Bed-set
Layer
Soil
Epiclastic
Juveniles (main comp)
>Dense
>Vesicular
Sorting
psr ms ws vs cs ms
Bedding, structures & others
C-shape
a sa sr rd wr
Observations
Interpretation
0.3
Burrell
avg. 0.45
Waingongoro-Puniho
Te Popo
0.7
G-III
1.2
1.0
Kp
MrP-I
Grey PDC-II
3rd Order Unconformity
MC
CR
MF
MkP-IV,-V
1.6
Maketawa II
1.9
Grey PDC-I
meters
FA FL B
CA CL
Layer 1 consists of white, pumiceous ash and free crystals. Layer 2 comprises very vesicular (~57-77 vol.%; Platz et al. 2007), moderately crystalline (~26-30 vol.%) pumice lapilli; dense, porphyritic grey-bluish and few orange-altered lithic lapilli. Layer 3 is similar to Layer 1
Four Members: Waingongoro, Newall, Waiweranui, Puniho (Platz 2007); separated by paleosols or weathered ash. They comprise often lensing deposits of light grey or brown-altered lithic and few pumiceous ash, supporting grey to dark-grey dense lithics, pumice lapilli and few altered-lithic lapilli. Desposits become finer and faint-parallel to -cross-stratified downslope. They may also thicken laterally, westwards.
Layer 1: pinching, dense lithic ash and free crystals with few lineaments of lithic lapilli. Layers 2, 4 and 6 consist of vesicular (~42-46 vol.%), moderately crystalline (~15-18 vol.%) pumice lapilli and bombs (60-87 vol.%); and dense and/or poorly vesicular (<15 vol.%), grey-bluish juveniles and altered-red or -orange porphyritic lithics (12-33 vol.%). Lithics mainly concentrate in base and top levels of layers 2, 4 and 6. Layer 5 is a fine pumiceous ash separating layers 4 and 6. Layers 3a and 3c consist mostly of lithic (~45 vol.%) and pumice (~43 vol.%) lapilli, in a matrix of whitish pumiceous ash (~30-34 vol.%). Layer 3b is clast-rich, having ~60 vol.% lithic and 30 vol.% pumice lapilli, and only ~10vol.% of a crystalline ash matrix. Laterally, layers 3a-3c become a single pinching bed (Layer 3) of withish fine ash in different proportions, supporting fine pumice and lithic lapilli.
Pinching grey lithic ash, supporting free crystals and diffuse fine pumice and lithic lapilli on top.
Very vesicular (~58-64 vol.%), crystal-rich (~25-30 vol.%) brownish pumice lapilli and scarce dark-grey lithic lapilli.
Diffuse bed of ash, supporting pumice and lithic lapilli, often scattered within soil.
Layer 1: Pinching deposit of pink and grey-bluish, dense, lithic ash and free crystals. Layer 2: Grey, fine to coarse lithic and free crystals-rich ash; supporting dark grey, dense, porphyritic, andesitic lithic lapilli and blocks of up to 1 m in diameter. Layer 3 consists of the same lithic components of layer 2, but lacking lapilli and block-size clasts, which makes an abrupt contact in between both layers. Laterally and downslope, layers 2- 3 pinch out, become fine-grained and strongly parallel- and cross-stratified with charcoal-bearing, reverse graded, fine lithic lapilli lenses.
Weathered medium sands and heterolithic fine-coarse pebble gravels.
Diffuse bed of poorly vesicular (~18-22 vol.%) porphyritic, dark grey/black lithic and scoria lapilli (Unit-2 of Turner et al. 2008b)
Layer 1: Purplish-grey lithic and pumiceous ash. Layer 2: Dense, grey andesite lithic lapilli (60 vol.%) and grey-brownish pumice lapilli (40 vol.%; CR-Unit 1 of Turner et al., 2008b).
Dark-grey and brown, vesicular and dense-microvesicular (~22-27 vol.%), moderately crystalline (~19-24 vol.%), scoria and pumice lapilli, and scarlet-red, dense, porphyritic lithic lapilli.
Two bed-sets separated by weathered ash; consisting of grey dense lithic ash and free crystals supporting charcoal-bearing, top and middle pinching beds of dense, porphyritic lithic and scarce pumice lapilli.
Layer 1: Yellowish, pumiceous ash supporting few free crystals and pumice and lithic lapilli. Layer 2: Poorly vesicular, (~35 vol.%), crystalline (~28 vol.%) pumice lapilli and grey/dark-grey lithic lapilli. Layer 3: Low-erosive, grey, lithic and less pumiceous ash, supporting grey lithic and pumice lapilli and clast-supported pumice lapilli lenses. Layer 4: Similar to Layer 1 but fine-grained. Layer 5: Similar to Layer 2. Laterally, layer 2 merges with lenses of layer 3 to become a single clast-supported bed; layer 3 pinches out until disappear and layer 4 expands.
Layer 1: Grey, dense lithic ash supporting grey, dark-grey, grey-bluish, altered-orange and -whitish, dense lithic lapilli. Layer 1 in-fills shallow erosive channels. Layer 2: A yellow-altered lensing ash, supporting aligned, very fine lithic lapilli, underlies layer 2; which consists of grey, dense lithic ash, supporting lineaments of grey and dark-grey -black lithic lapilli that make most of the layer. Laterally, layers 1-2 pinch-out and become strongly parallel-/ cross-stratified, but the difference in grain-size in between both layers makes the contact very distinctive.
Interpretation
C-PDC
Fallout
BAF
BAF
BAF
BAF
PDC
Fallout
Fallout
C-PDC
Fallout
BAF
BAF
PDC
BAF
Major Time-break
Fallout
Fallout
PDC
Fallout
BAF
BAF
Fallout
C-PDC
C-PDC
Fallout
C-PDC
BAF
BAF

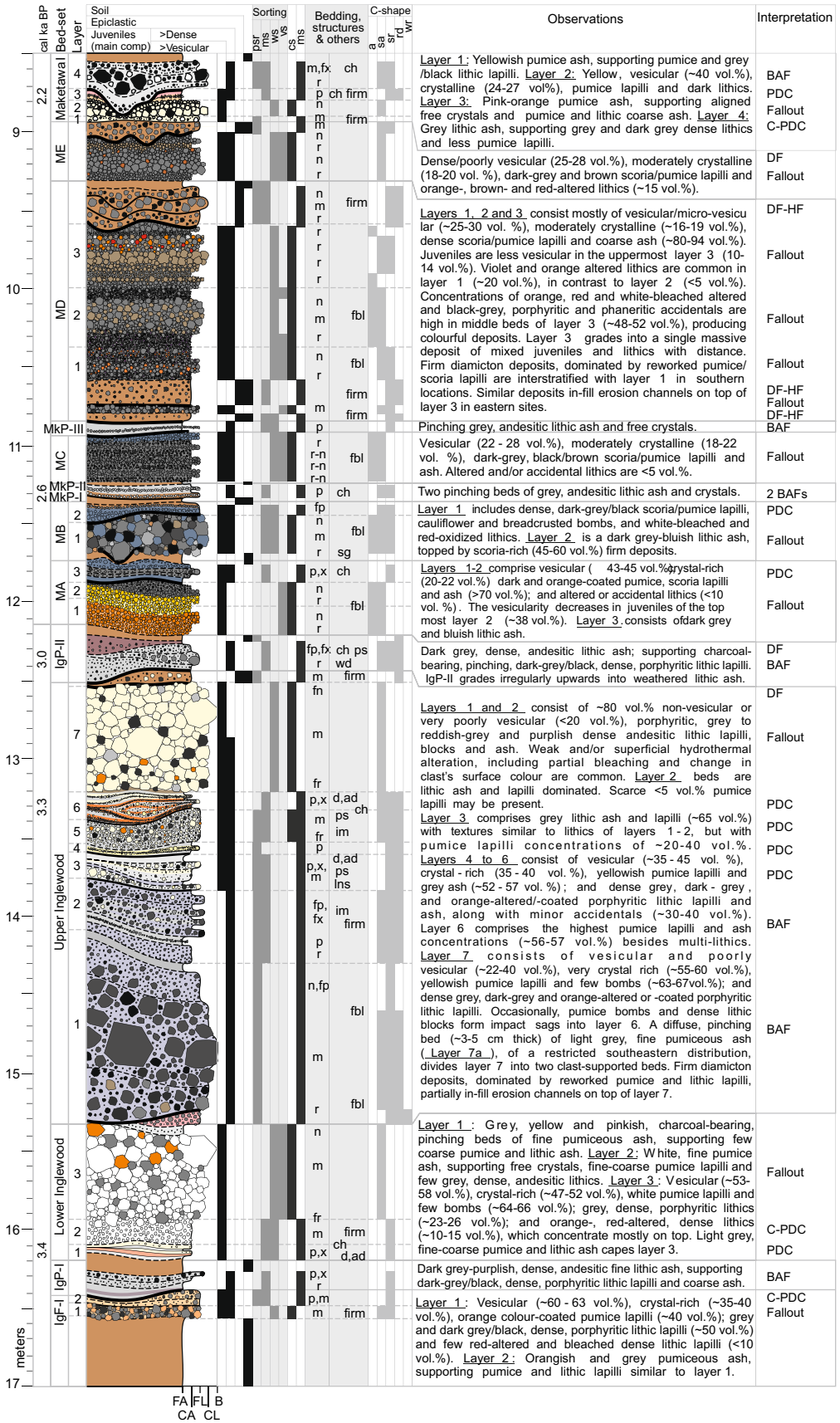

Fig. 3 (continued)

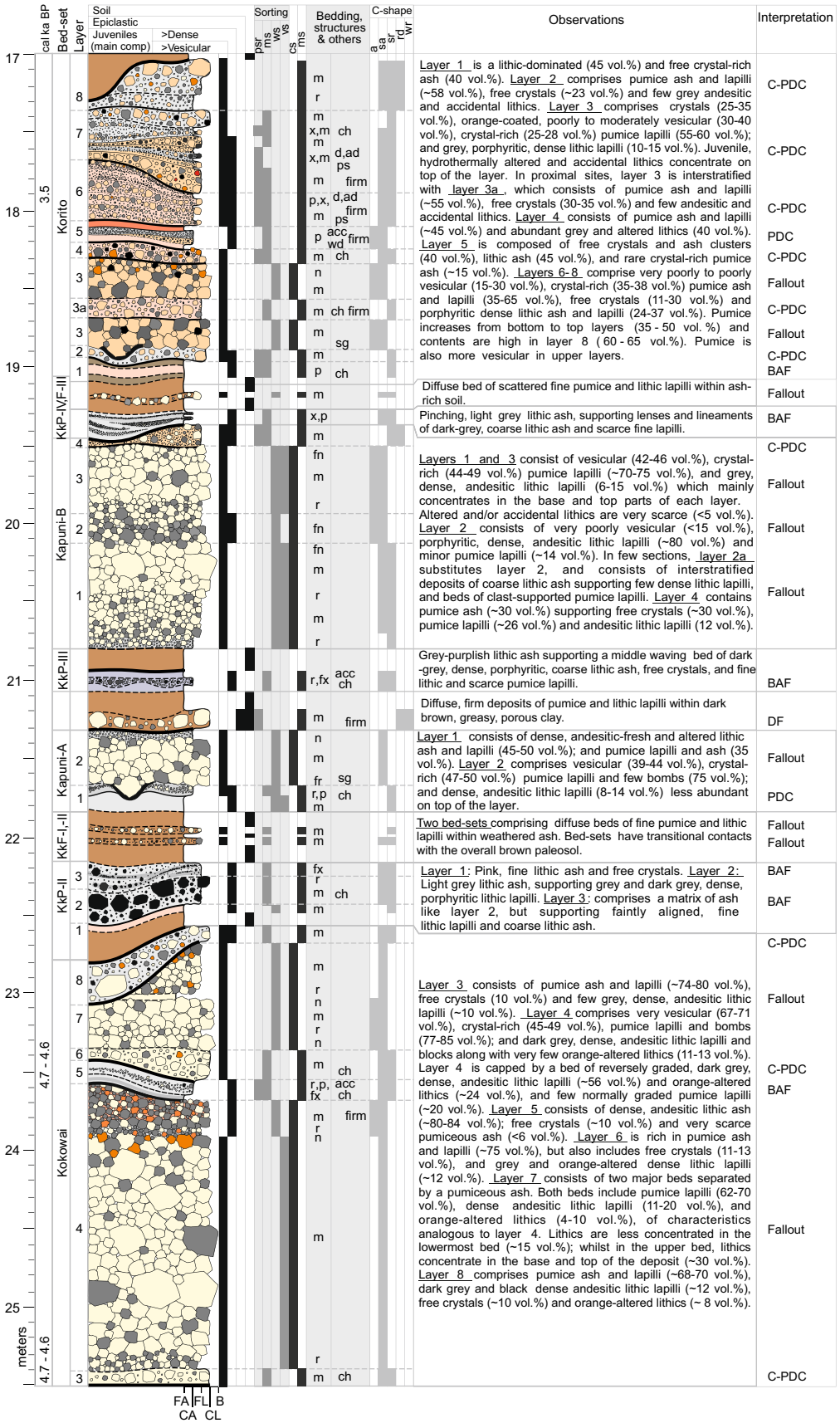

Fig. 3 (continued)

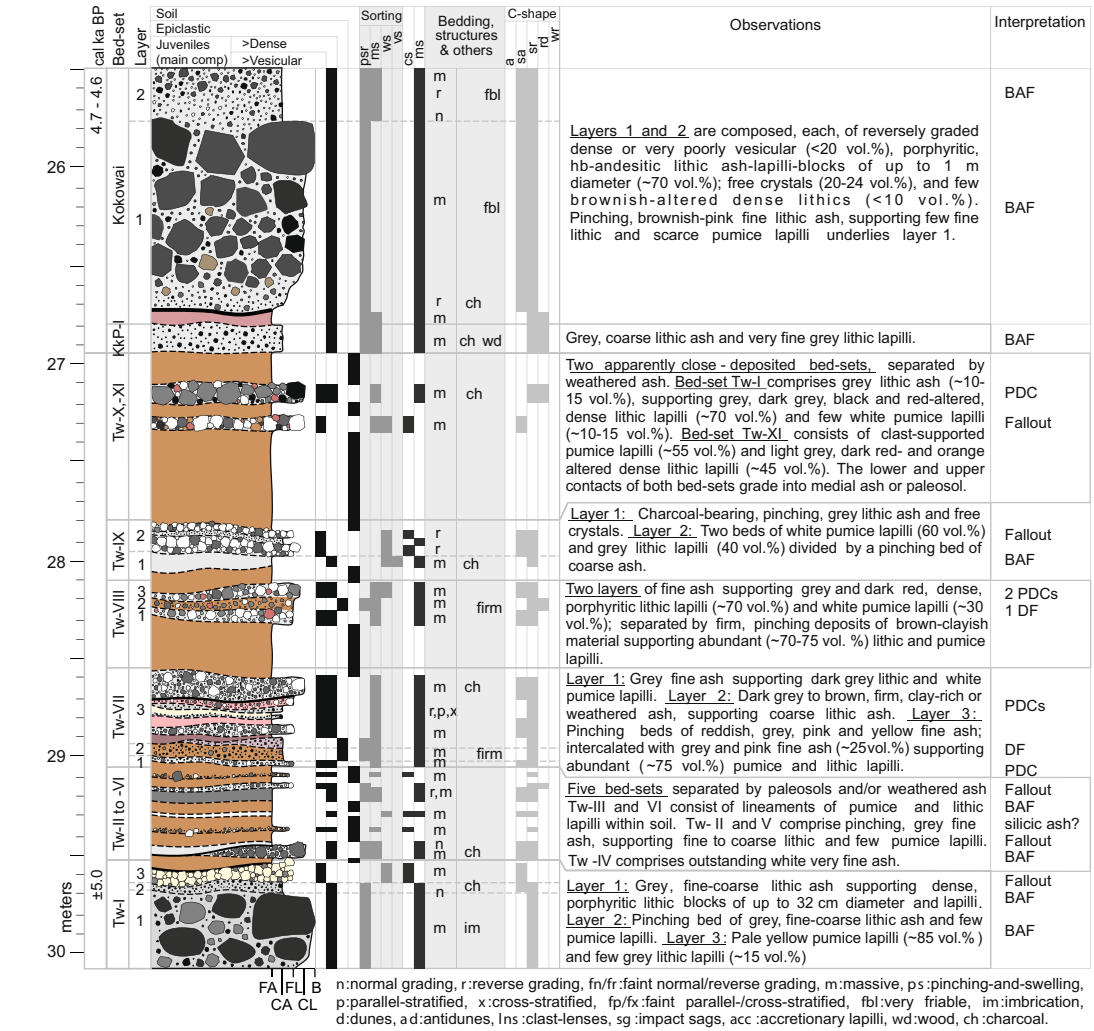

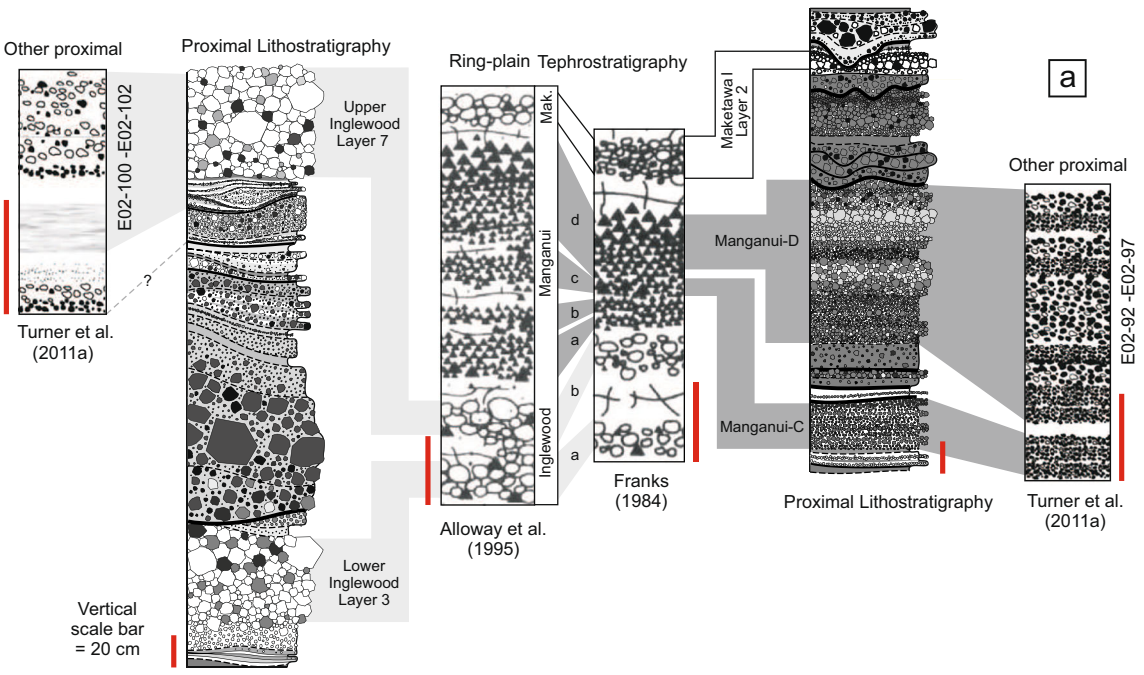

Fig. 3 (continued)

◀ **Fig. 3** Composite stratigraphic log of the late-Holocene proximal pyroclastic sequence of Mt. Taranaki. Members of the Manganui Formation (i.e. Manganui A to G) are abbreviated *MA…MG*. *CR* Curtis Ridge Lapilli bed-set (Turner et al. 2008b). Main juvenile pyroclasts are indicated (dense-vesicular). *Solid lines* indicate sharp contacts; *bold solid lines* indicate sharp erosive (often angular) contacts; *dashed lines* indicate transitional contacts. Grain size simplified from White and Houghton (2006): *FA* fine ash, CA coarse ash, *FL* fine lapilli, *CL* coarse lapilli, *B* blocks/bombs. Sorting: poor (*psr*), moderate (*ms*), well (*ws*) and very well sorting (*vs*) from Cas et al. (2008). Clast (*cs*) and matrix-support (*ms*) framework and angular (*a*), sub-angular (*sa*), sub-rounded (*sr*), rounded (*rd*) and well-rounded (*wr*) clast-shape are indicated. *DF* debris flow, *C-PDC* column-collapse pyroclastic density current, *BAF* block-and-ash flow, *PDC* undefined pyroclastic density current. **a** Comparison of a segment from the previous ring plain and distal tephrostratigraphy with the equivalent proximal lithostratigraphy of this work and a few earlier studies. See text and Table 1 for ^{14}C age references

single or multiple *layers*. The term Tephra Formation is here only referred for citation of deposits previously named and described in that way. We prefer not to use a genetic terminology for the lithostratigraphic nomenclature, considering potential lithofacies variations with distance and following the recommendations of Salvador (1994).

The upper and lower contacts of a bed-set are given by the embedding fine-ash-dominated paleosols, thick medial ash deposits (mostly centimetres to tens of centemetre-thick deposits of moderately weathered, massive fine-medium ash), and the base and top, respectively, of deep-erosion surfaces (including paleochannels). All these features suggest quiescence periods in the eruptive deposition.

Fine-grained, mud- and sand-dominated hypercon centrated flow deposits (mostly tens of centemetre thick) may represent time breaks in the volcanic activity when they show signs of weathering and paleosol development. By contrast, debris- and hyperconcentrated flow deposits containing abundant juvenile clasts from the underlying pyroclastic deposit indicate only short intervals or may represent deposits of syn-eruptive events. In addition, one 3rd-order unconformity was identified (Fig. 2), demarking a significant repose period, which can be traced in a ~10–15-km arc around the eastern volcano flanks.

Following the terminology of Fisher and Schmincke (1984), each of the lithostratigraphic bed-sets analysed could be products of a definable *eruption* bounded by paleosols that suggest a significant period without eruptive activity. Thereafter, each of the layers within a bed-set, separated by sharp, gradational and/or locally mildly erosive boundaries that suggest no evident pause in deposition (e.g. contacts given by sharp differences in grain-size, clast framework and/or bed structure), represents an *eruption unit* deposited from an individual fallout, pyroclastic density current (PDC) or a lava flow. An eruption consisting of a single eruption unit will be referred as an *eruption event*; whereas an eruption consisting of multiple-eruption units will be referred as an *eruption episode*. In this latter case, each of the composing eruption units could be interpreted as the accumulation of an eruption phase.

Radiocarbon dating

Samples of charcoal from distinct bed-sets were collected for radiocarbon (^{14}C) dating, and sites of earlier ^{14}C dates (e.g. Turner et al. 2008b, 2011a) were reviewed where sampling sites were clearly known. Six new dates were obtained using the accelerator mass spectrometer technique at the Radiocarbon Dating Laboratory of Waikato University, New Zealand (Table 1). Results were determined following Stuiver and Polach (1977), based on the Libby half-life of 5568 years with correction for isotopic fractionation. All ages were calibrated using OxCal 4.2 (Bronk-Ramsey 2009). The southern hemisphere atmospheric curve was employed (Hogg et al. 2013). The ^{14}C dates from previous works were also calibrated in the same manner for consistency.

The late-Holocene eruption records of Mt. Taranaki

In the proximal exposures on Mt. Taranaki, 53 bed-sets were identified (Fig. 3), each one capped by 10–20-cm-thick ash-rich paleosols or weathered ash deposits. Among these 53 bed-sets, 36 underlie a 3rd-order unconformity which is traceable over the eastern flank of the volcano. Based on the nearest stratigraphically underlying 7.5-cal ka B.P. debris-avalanche deposits (Neall 1979; Zernack et al. 2011), these 36 bed-sets could be considered part of the Opua Formation defined by Neall and Alloway (2004). Nevertheless, it was not possible to corroborate this stratigraphic position, because the base of the stratigraphic sequence studied here remains unknown, and there are not enough outcrops to construct mappable units. In contrast, the uppermost ~3- to >1.2-cal ka B.P. bed-sets are interdigitated with the well-recognized and mappable Manganui Formation (Whitehead 1976; Alloway et al. 1995), which includes seven bed-sets sourced at Fanthams Peak, as we demonstrate below. Another ten pyroclastic bed-sets (~1.2 cal ka B.P. to AD 1655) overlying the 3rd-order unconformity are Mt. Taranaki sourced and, given their better exposure, could be grouped and mapped as part of the Maero Formation (cf. Neall 1979; Neall et al. 1986; Cronin et al. 2003; Platz 2007).

A significant feature within the reconstructed stratigraphic sequence is a 3rd-order unconformity (i.e. a surface of erosion that is extended over a specific sector of the volcano; Lucchi et al. 2013), which consists of an irregular disconformity lying, with a sharp-erosive contact, on top of <1.6 cal ka B.P. deposits of the Manganui-G Member (q.v. Manganui Formation) and the Curtis Ridge bed-set (cf. Turner et al. 2008b) in southeastern sections (e.g. sections F–G; Figs. 1

Table 1 Radiocarbon dating of material from proximal sections of Mt. Taranaki

Lab code	Location	Section	Material		a BP	1 s	cal a BP	2 s	Bed-set/member
This work									
Wk-39445	Maketawa Hut	N	Charcoal	–[a]	2223	25	2210	60	Maketawa I
Wk-19168	York track	A	Log	–[a]	2277	39	2240	55	Maketawa I
Wk-19169	Kaupokonui stm	B	Punga log	–[a]	2515	38	2560	100	MkP-I
Wk-39446	Maketawa Hut	N	Charcoal	–[a]	2946	25	3040	55	IgP-II
Wk-39436	Holly Hut 1	X	Charcoal	–[a]	3115	25	3280	50	Upper Inglewood
Wk-39437	Camphouse	S	Charcoal	–[a]	3180	29	3350	55	Lower Inglewood
Wk-39439	Kokowai	W	Charcoal	–[a]	4140	25	4630	90	Kokowai
Wk-39440	Kokowai	W	Charcoal	–[a]	4213	25	4710	70	Kokowai
Calibrated from previous works									
Wk-11586	Maero stream	–	Flakes	Cronin et al. (2003)	878	39	745	40	Te Popo
Wk-16391	Little Maketawa	M	Charcoal	Turner (2008)	1130	34	995	40	Grey PDC-III
Wk-16390	Little Maketawa	M	Charcoal	Turner (2008)	1739	35	1615	50	Maketawa II
Wk-16392	Little Maketawa	M	Charcoal	Turner (2008)	1989	45	1900	60	Grey PDC-I
NZ-3886C	Stratford Plateau	H	Charcoal	Neall and Alloway (1986)	1934	70	1830	90	Grey PDC-I
Wk-16397	North Egmont Rd	T	Charcoal	Turner (2008)	2217	36	2200	70	Maketawa I
Wk-16393	Holly Hut 1	X	Charcoal	Turner (2008)	3102	37	3270	60	Upper Inglewood
Wk-16395	Okahu stream	–	Charcoal	Turner (2008)	3362	37	3545	55	Korito
Wk-16396	Okahu stream	–	Charcoal	Turner (2008)	4429	45	4980	100	Undefined PDC

Original age of 1990 ± 70 a BP (Neall and Alloway 1986) was recalculated for the Libby half-life of 5568 years. All ages were calibrated using OxCal 4.2 of the Oxford Radiocarbon Accelerator Unit (Bronk-Ramsey 2009). The Southern hemisphere atmospheric curve (SHCal13) of Hogg et al. (2013) was employed

[a] Uncalibrated radiocarbon ages in this work (and Lab codes Wk-) were determined by the Radiocarbon Dating Laboratory of the University of Waikato, New Zealand, using the accelerator mass spectrometer technique. Results correspond to a conventional age or percent modern carbon (pMC) following Stuiver and Polach (1977). This is based on the Libby half-life of 5568 years with correction for isotopic fractionation applied

and 2), and most commonly on top of deposits of the Manganui F Member in the northeast (of the Manganui Formation). In few northeastern locations (e.g. sections Q and R; Figs. 1 and 2), the unconformity cuts as a ~30° angular contact down into >2.2 cal ka B.P. deposits of the Maganui E Member (q.v. Manganui Formation).

Deposits associated with the unconformity consist of up to 70-cm-thick, massive, poorly sorted, fine to medium sands supporting heterolithic fine to coarse pebbles (Fig. 3), capping and in-filling erosion surfaces (e.g. paleochannels). These deposits generally exhibit a flat top, grading into ~10-cm-thick paleosols, or a sharp contact with capping lithic breccias and fine lithic ash deposits (i.e. the Grey PDC-II Member, Fig. 3). Applying ^{14}C dating of bed-sets below and above indicates that the unconformity occupied an interval between ~1.6 and 1.2 cal ka B.P. (calibrated from Neall and Jansen 1984 and Turner 2008).

In general, deposits of the different bed-sets of Mt. Taranaki comprise white-yellow pumice, grey porphyritic juvenile lithics, altered lithics and accidental clasts, containing crystals of plagioclase, hornblende, Fe–Ti oxides, ortho and clinopyroxene and minor biotite consistent with basaltic-andesitic and andesitic compositions reported elsewhere (53.5–60 wt.% SiO_2; e.g. Neall et al. 1986; Price et al. 1992; Stewart et al. 1996; Turner et al. 2011b; Platz et al. 2007, 2012). In contrast, the basaltic and few basaltic-andesitic deposits of the Manganui Formation (48–53 wt.% SiO_2; Price et al. 1992; Stewart et al. 1996; May 2003; Turner et al. 2011b) comprise mostly grey and dark-grey porphyritic juvenile lithics, few dark-grey scoria and dark-brown pumice, bearing ortho and clinopyroxene, hornblende, Fe–Ti oxides and olivine crystals.

Below, we describe the thickest and most readily followed deposits of the stratigraphic sequence in depositional order (Figs. 2 and 3), separately grouping bed-sets identified from the Mt. Taranaki summit vent, versus those from Fanthams Peak.

The Mt. Taranaki Lithosome

The oldest deposits studied in this work include 11 bed-sets recognized on the northern flanks of Mt. Taranaki. Bed-sets Tw-I, Tw-VII and Tw-IX to Tw-XI contain the thickest deposits of the suite (Fig. 3) and are likely associated to fall deposits within the Tariki and Waipuku Tephra Formations mapped by Alloway et al. (1995) on the ring plain. They are

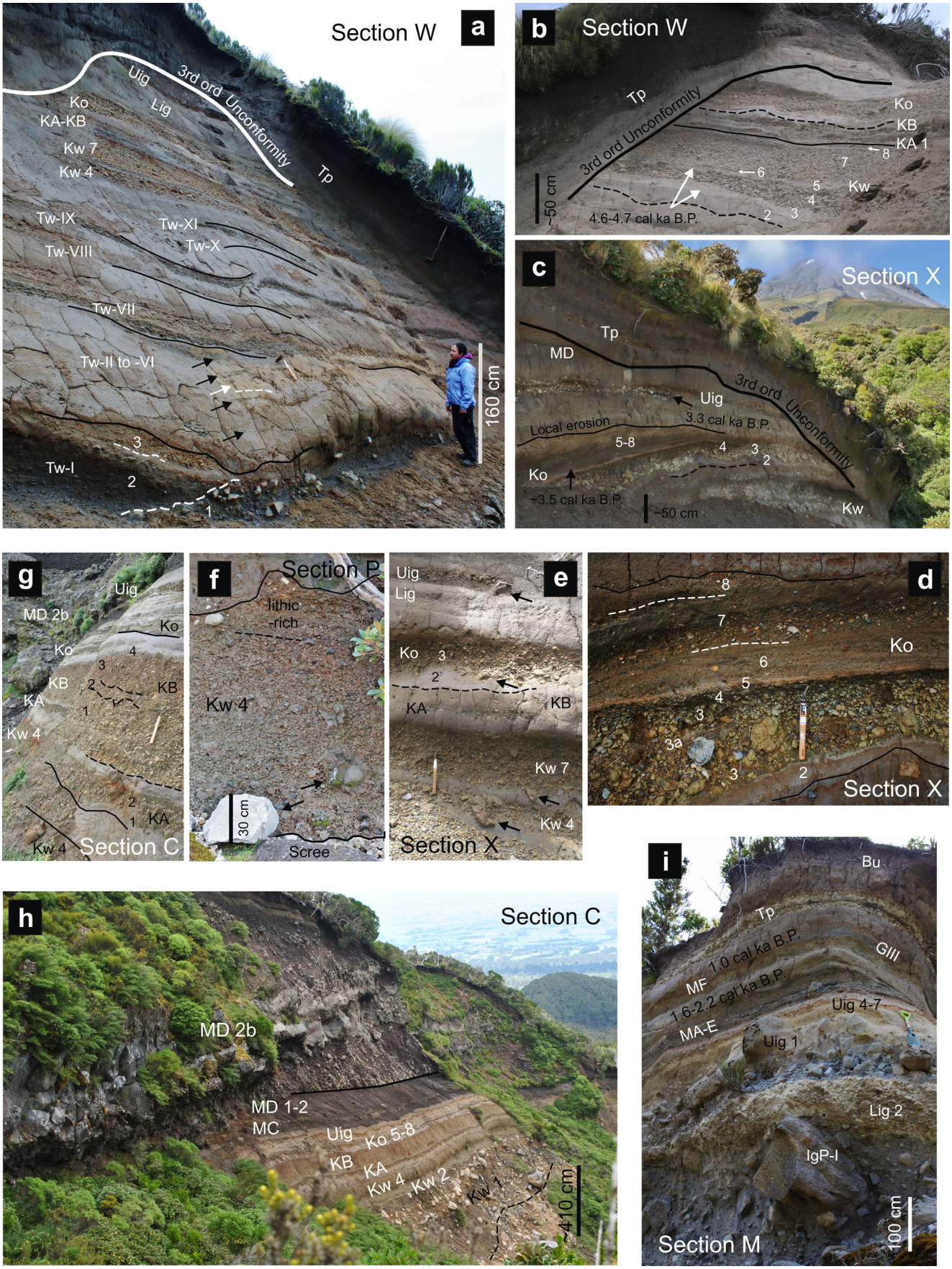
a
Section W
Uig
Lig
3rd ord Unconformity
Tp
Ko
KA-KB
Kw 7
Kw 4
Tw-IX
Tw-XI
Tw-X
Tw-VIII
Tw-VII
Tw-II to -VI
Tw-I
160 cm
b
Section W
Tp
3rd ord Unconformity
Ko
KB
KA 1
~50 cm
4.6-4.7 cal ka B.P.
Kw
c
Section X
Tp
MD
3rd ord Unconformity
Uig
3.3 cal ka B.P.
Local erosion
5-8
Ko
~3.5 cal ka B.P.
~50 cm
Kw
d
Ko
Section X
e
Uig
Lig
Ko
KA
KB
Kw 7
Kw 4
Section X
f
Section P
lithic
-rich
Kw 4
30 cm
Scree
g
Uig
MD 2b
Ko
KB
KA
Kw 4
Section C
h
Section C
MD 2b
MD 1-2
MC
Uig
Ko 5-8
KB
KA
Kw 4
Kw 2
Kw 1
~410 cm
i
Bu
Tp
MF 1.0 cal ka B.P.
1.6-2.2 cal ka B.P.
MA-E
GIII
Uig 4-7
Uig 1
Lig 2
IgP-I
Section M
100 cm

Fig. 4 (continued)

Fig. 4 Photographs showing the deposit features of representative late-Holocene bed-sets/members exposed at different eastern-flank sections of Mt. Taranaki. Bed-sets/members are Tw-I to Tw-XI, *Kw* Kokowai, *KA* and *KB* Kapuni A and B, *Ko* Korito, *Lig* Lower Inglewood, *Uig* Upper Inglewood, *MA to MF* Manganui A to F, *MkI and MkII* Maketawa I and II, *CR* Curtis Ridge, *Kp* Kaupokonui, *GI to GIII* Grey PDC-I to PDC-III, *Tp* Te Popo, *Bu* Burrell. **a** Deposits of the ~5-ka bed-sets and stratigraphic relationships with younger 4.7–3.3 cal ka B.P. deposits. **b** Complete Kw bed-set. Radiocarbon (^{14}C) dating of charcoal from layers 3 and 5–6 is indicated. **c** Northern stratigraphic relationships between different 4.7–3.3 cal ka B.P. and younger ~2.6–0.7 cal ka B.P. bed-sets. ^{14}C-dated layers from bed-sets Ko and Uig are indicated. **d** Zoom of the Ko. **e** Impact sags produced by pumice bombs of different 4.7–3.3 cal ka B.P. bed-sets. **f** Fall deposits of the Kw layer 4. Bombs and blocks are signalled. **g** Fall deposits of bed-sets KA and KB separated by weathered ash. **h** Block-and-ash flow and fall deposits of the Kw constitute the base of the exposed section. Lava flows (MD 2b) from Fanthams Peak erode fall deposits of the MD. **i** Stratigraphic relationships and ^{14}C-dated deposits of 3.4–0.3 cal ka B.P. bed-sets. Block-and-ash flow deposits underlying layer 2 of the Lig bed-set make the base of the exposed section. Notice block-and-ash flow deposits of the Uig (layer 1). **j**–**l** Deposit features of the Uig in southeastern-northeastern locations. Notice lithofacies transitions of layer 6 and ^{14}C dating of charcoal from bracketing bed-sets. **m** Deposits of the <3.0–2.2-cal ka B.P. MA to MD Members and other bracketing and/or younger deposits. **n** Zoom of the MC-MD Members and bracketing debris-flow deposits. **o** Zoom of the MA-MC members. Notice the cauliflower bomb of the MB member deforming deposits of the MA. Notice grey-lithic ash deposits of bed-sets MkP-I and MkP-II (not labelled), which pass laterally into ^{14}C-dated 2.6 cal ka B.P. lithic breccias. **p**–**t** Deposit features and lithofacies transitions of the Mk II. **s** Notice the commonly overlying deposits of the MF and their distinctive scarlet-red lithics. **t** Notice deposits of the GI bed-set. **u**–**w** Deposit features of the Tp. Notice ash deposits of layer 1 (*Tp1*), which correlate with western 0.7 cal ka B.P. lithic breccias. Cross- (*x*), parallel- (*p*) or faint parallel/cross-stratified (*fp/fx*) and massive (*m*) deposits. Spade is 70.5-cm long, large scraper is 32.5-cm long and small scraper is 20-cm long. See text and Table 1 for ^{14}C age references

poorly exposed in only two adjacent sections: W and X (Figs. 1 and 2) and charcoal fragments were too small or degraded to perform ^{14}C dating, thus their estimated age is ~5 ka, based on the ^{14}C age of the closest overlying bed-set (i.e. ~4.7–4.6 cal ka B.P. Kokowai, Table 1), and on their approximate correlation with western ~5 cal ka B.P. lithic breccias (Turner 2008; Figs. 2 and 3).

Bed-sets Tw-I to Tw-VII

The oldest Tw-I bed-set comprises three layers (Figs. 3 and 4). The basal contact of the lowermost layer (layer 1) is exposed within an inaccessible ~100-m vertical valley wall. The accessible part of this layer is a massive, poorly sorted lithic breccia, tens of metres thick and dominated by dense, porphyritic andesitic blocks and lapilli (at times imbricated) within an ash matrix. This deposit is capped by layer 2, which comprises normal-graded, poorly sorted lithic ash of similar composition to the underlying deposit. The uppermost layer 3 is a distinctive mantling bed of massive, well-sorted, clast-supported pumice lapilli (Figs. 3 and 4).

Each of the Tw-II to Tw-VII bed-sets comprises deposits with transitional or diffuse contacts within encapsulating lower and upper paleosols (Fig. 3). Tw-II and Tw-V comprise massive, moderately to poorly sorted pinching beds of ash supporting lithic lapilli. Tw-IV comprises diffuse, massive and well-sorted very fine white ash. Tw-III and Tw-VI consist of diffuse and often lensing, massive, moderately sorted beds of pumice and lithic ash or lapilli. Bed-set Tw-VII consists of two very similar layers (layers 1 and 3) comprising several parallel, cross-stratified and massive, moderately sorted pinching beds of ash supporting pumice and lithic lapilli; divided by layer 2, which is a massive firm brown ash supporting abundant coarse ash and few lithic lapilli.

Bed-sets Tw-VIII and Tw-IX

Bed-sets Tw-VIII and Tw-IX lie over ~30-cm-thick paleosols and weathered ash developed on top of bed-set Tw-VII and are separated by transitional contacts with ~15-cm-thick weathered ash deposits. At its maximum thickness, bed-set Tw-VIII comprises two layers of massive, moderately sorted pumice and lithic lapilli within an ash matrix, divided by a layer of firm, massive and poorly sorted pinching clay-rich ash (Fig. 3). These three layers merge rapidly into a single bedded deposit, which is the most common appearance. Bed-set Tw-IX consists of two layers (Fig. 3). Layer 1 is a charcoal-rich, massive, well-sorted pinching lithic ash, and layer 2 consists of two reverse-graded, well-sorted and clast-supported mantling beds of distinctive white pumice lapilli, divided by a pinching bed of pumice ash.

Bed-sets Tw-X and Tw-XI

Bed-sets Tw-X and Tw-XI overlie ~50-cm-thick paleosols and weathered ash developed on top of Tw-IX (Fig. 3) and are separated by <10-cm-thick weathered ash deposits with sharp contacts in between. Tw-X comprises massive, moderately to well-sorted, clast-supported, mantling pumice and lithic lapilli deposits. Tw-XI consists of a massive, moderately sorted, pinching-swelling bed of lithic-rich lapilli with an interstitial lithic ash matrix, bearing rare charcoal twigs.

The Kokowai bed-set

The Kokowai bed-set (Kw) contains the thickest and coarsest pyroclastic deposits studied in this work. A sharp contact with up to 30-cm-thick paleosols developed on top of weathered ash deposits separate the Kw from older bed-sets (Fig. 3). The Kw comprises eight layers (Fig. 3) exposed in sections along the eastern flank of the volcano, which are best seen at the Kokowai section (section W; Figs. 1 and 2).

The most distinctive deposits of the Kw correspond to layers 1, 4 and 7 (Figs. 3 and 4). Layer 1 consists of up to 10-m-thick, reverse-graded, poorly to moderately sorted lithic breccias on the volcano southeast flanks, containing porphyritic andesitic blocks of up to 1-m-diameter through to coarse lapilli. Layers 4 and 7 contain almost exclusively massive or stratified, well- and very well-sorted, clast-supported, crystal-rich pumice lapilli beds. Layer 4 reaches up to 1.7-m thick at northeast exposures (Fig. 4), where it is capped by a bed of dense-lithic lapilli. The remaining layers comprise poorly to moderately sorted, matrix-supported pinching beds of ash, rich in either pumice lapilli or andesitic lithic ash and lapilli.

^{14}C dating of charcoal fragments within layers 3 and 6 at section W indicates an age of 4.7–4.6 cal ka B.P. for the Kw (Table 1), which approximately correlates with deposits described by Turner (2008) at Waipuku Stream and Wilkies Pools sections (i.e. deposits M05-69 and M06-54, respectively; sections J and ~D, Figs. 1 and 2). These ages suggest that the Kw lies stratigraphically above ~5 ka B.P. ring-plain deposits of the Tariki Tephra Formation mapped within soils east and south of Mt. Taranaki by Alloway et al. (1995).

Bed-sets KkF-I and KkF-II

Two bed-sets (i.e. KkF-I and KkF-II) are separated in between by an intervening ~5–8-cm-thick paleosol with diffuse contacts (Fig. 3). In southeastern locations, they lie over ~15-cm-thick paleosols developed on top of weathered ash from older deposits (e.g. sections C and D, Figs. 2 and 3). Each bed-set consists of a single massive, moderately sorted and very thin bed of fine pumice and lithic lapilli; which might stratigraphically correlate with the Mangatoki Tephra (~4.4 ka B.P.) mapped by Alloway et al. (1995) in ring-plain locations.

The Kapuni A bed-set

The Kapuni A bed-set (KA) lies with a gradational contact over ~10–40-cm-thick weathered ash deposits on top of bed-sets KkF-I, KkF-II or KkP-II at southeast sections (Figs. 2 and 3). The KA includes two layers (Fig. 3), with the best exposure near Hooker Shelter (section C, Figs. 1 and 2). Layer 2 is the thickest (Figs. 3 and 4) and comprises a massive, well-sorted and clast-supported bed of mostly crystal-rich pumice lapilli, which correlates with >3.8 ka B.P. pumice beds (i.e. between M05-67 and M05-68) described by Turner (2008) at Waipuku stream (section J, Figs. 1 and 2).

The Kapuni B bed-set

The Kapuni B bed-set (KB) lies with either sharp or gradational contact above a well-developed ~15-cm-thick paleosol, or at Wilkies Pools section, directly over ~20-cm-thick lithic ash deposits (i.e. bed-set KkP-III; Fig. 3) and onto the KA bed-set (section D, Figs. 1 and 2). The KB bed-set consists of at least four layers (Fig. 3) exposed on the volcano's southeastern, northeastern and northern flanks, best observed at section C (Figs. 1 and 2). Layers 1 and 3 are the most distinctive as near-identical reverse-graded to massive, well- to very well-sorted, clast-supported beds (Fig. 4), comprising mostly crystal-rich pumice lapilli and also lithic lapilli. The latter mainly concentrate at the base and top levels of each layer. Layer 2 separates the pumice layers 1 and 3 and consists of a reverse to normal-graded, well-sorted and clast-supported bed, dominated by dense, porphyritic hornblende-rich andesitic lithic lapilli (Fig. 3). In northeastern sections, layer 2 is replaced by multiple reverse-graded and clast-supported beds of pumice ash and lapilli, interstratified with massive beds of ash supporting pumice and andesitic lithic lapilli.

Based on its stratigraphic position, the KB correlates with one or more <3.8 ka B.P. unnamed pumice beds described by Turner (2008) on the eastern flanks at section J (i.e. M05-66 and M05-67; Figs. 1 and 2).

The Korito bed-set

The Korito bed-set (Ko) lies with a transitional contact over ~10–30-cm-thick paleosols developed on weathered ash (Fig. 3) on top of different deposits depending on the location (Fig. 2). The Ko deposits are unique in Taranaki's studied <5 ka sequence due to their varied lithologies and very distinctive yellow- to red-orange-coloured pumice. This bed-set is a useful marker horizon in proximal exposures.

The Ko comprises nine layers (1–8 and 3a; Fig. 3), best observed at Kokowai and Holly Hut 1 sections (sections W and X, Figs. 1 and 2). Layer 3 contains two massive, well-sorted and clast-supported pumice-dominated lapilli beds, which are separated by matrix-supported deposits (layer 3a) in northern exposures (Figs. 3 and 4). Hydrothermally altered and accidental dense lithics are common at the normal-graded top part of layer 3 (Fig. 3). In southern sites, only a single lapilli bed is seen.

Layer 5 is an unusual orange to pink-coloured, parallel-stratified, pinching and fine-grained deposit, useful to correlate the Ko (Figs. 3 and 4). This layer is firm, appears cemented and is composed of particle clusters (in some cases accretionary lapilli) of highly angular, dense-lithic and loose-crystal ash and rare crystal-rich pumice ash, bearing common wood fragments. Layers 6–8 are the most widely distributed and thickest deposits of the overall bed-set. They comprise intercalated cross-, parallel-stratified and massive, poorly to moderately sorted, pinching-swelling beds of ash and lapilli (Figs. 3 and 4), made up of very poorly to poorly vesicular, crystal-rich pumice and porphyritic lithics. Charcoal twigs are common in layers 7–8.

Some of these layers are traceable ~8 km northwards, across the neighbouring Pouakai volcano and down to Korito road (Figs. 1 and 2). With distance, layers 5–7 merge, become finer grained, and together with lensing or scattered pumice lapilli of layers 3 and 8 correlate with the Korito Tephra mapped by Neall (1972). On the ring plain, Alloway et al. (1995) assigned maximum and minimum ^{14}C ages of 4.1 and 3.5 ka B.P. for the Korito Tephra from coastal cliff exposures, ~42 km northeast of Mt. Taranaki and suggested that the silicic ~3.9 ka B.P. Stent Tephra (sourced from the TVZ; Alloway et al. 1994) should overlie the Korito Tephra. By contrast, Turner (2008) obtained an ^{14}C age of 3.5 cal ka B.P. (Table 1) for charcoal within a cross-stratified and lithic-rich 'surge' deposit at Okahu Stream, northwest of Mt. Taranaki, which correlates with layer 6. Ages of underlying Kokowai and overlying Upper Inglewood bed-sets (Table 1; Figs. 2 and 3) support the Turner (2008) age estimate of 3.5 cal ka B.P. for the Ko.

The Lower Inglewood bed-set

The Lower Inglewood bed-set (Lig) consists of three layers (Fig. 3) restricted to the east and north flanks of Mt. Taranaki, which are best seen at Waipuku stream, Little Maketawa and Camphouse sections (J, M and S, Figs. 1 and 2). In northern flank locations (e.g. section W, Fig. 2), sharp contacts with ~90- and 15-cm-thick deposits of weathered ash and paleosols separate the Lig from the Korito bed-set below and from the Upper Inglewood bed-set above, respectively (Figs. 2 and 4). On the northeast flanks of Mt. Taranaki (e.g. section S, Fig. 2), transitional contacts with similar weathered ash separate the Lig from bed-sets IgFC-I and IgPC-I below (Fig. 3).

Layers 2–3 comprise the most distinctive deposits. Layer 2 is a firm, massive, moderately to well-sorted pinching deposit of ash supporting white pumice and rare lithic lapilli. Layer 3 consists of mostly massive, well- to very well-sorted and clast-supported deposits, dominated by crystal-rich pumice lapilli with andesitic and altered lithics in upper deposit levels (Fig. 3).

At eastern-flank locations (e.g. section J and Lower Pembroke road, Figs. 1 and 2), layer 3 correlates with the Inglewood A bed of the Inglewood Tephra mapped by Alloway et al. (1995). An age of 3.6 ka B.P. was proposed by Alloway et al. (1995) for the Inglewood Tephra based on ^{14}C dating of peat and wood from encapsulating ring-plain and distal deposits. In this work, ^{14}C dating of charcoal within layer 1 at section S provides an age of 3.4 cal ka B.P. for the Lig (Table 1), which is consistent with under- and overlying bracketing bed-sets of 3.5 and 3.3 cal ka B.P., respectively (Table 1).

The Upper Inglewood bed-set

The Upper Inglewood bed-set (Uig) lies with sharp and erosive contacts directly upon deposits of the Lig in most northeastern areas (Fig. 3); whereas in southern and northern locations, transitional and sharp contacts separate the Uig from 10- to 20-cm-thick paleosols developed on top of bed-sets Lig, IgP-I, IgF-I or Ko (Fig. 2). The Uig is one of the most complex deposits seen during this study, with seven layers (Fig. 3) recording one of the largest explosive eruptions in Mt. Taranaki's history. Most layers are exposed across the entire eastern flank and, with its distinctive field appearance, form an ideal proximal stratigraphic marker (Fig. 2).

Layer 1 is a reverse-graded to massive and poorly sorted lithic breccia, containing dense grey and few hydrothermally altered porphyritic lithic blocks and coarse lapilli (Figs. 3 and 4). This layer laterally passes into massive, parallel- or cross-stratified pinching thin beds of ash and lapilli. Layers 2 and 3 are reverse-graded, parallel- and cross-stratified and poorly to moderately sorted lithic-dominated ash beds; that cap interfluves in a similar way to the lateral parts of layer 1; however, layer 3 additionally contains pumice lapilli in some areas. Layers 4–6 comprise overall poorly to moderately sorted and pinching-swelling, matrix-supported beds of multiple lithics and crystal-rich pumice (Figs. 3 and 4). They graduate vertically from basal, parallel-stratified, very thin beds of ash and lapilli (layer 4), into clast-rich massive beds of lapilli (layer 5), and finally, into upper parallel- and cross-stratified thin beds of ash showing occasional dune structures (layer 6). The uppermost layer 7 comprises a massive, well-sorted and clast-supported bed (Figs. 3 and 4) of crystal-rich pumice lapilli and dense, porphyritic lithic lapilli (Fig. 3).

From Holly Hut 1 section (section X, Fig. 1), layer 7 was traced northwards, down to Maude, Kent and Korito roads, where it correlates with the Inglewood Tephra mapped by Neall (1972). To the east flanks of Mt. Taranaki (e.g. sections F-I, Figs. 1 and 2), layer 7 correlates with the Inglewood B bed of the Inglewood Tephra defined by Alloway et al. (1995). In the present study, ^{14}C dating of ~30-cm-long charcoal logs within layer 6 at section X (Fig. 4) indicates an age of 3.3 cal ka B.P. for the Uig (Table 1), which is near identical to the ^{14}C date obtained by Turner (2008) in a correlative deposit. ^{14}C dating of charcoal within immediate over- and under-lying deposits at Maketawa Hut and Camphouse sections (N and S, Figs. 1 and 2) confirms maximum and minimum ages of 3.4 and 3.0 cal ka B.P., respectively (Table 1).

The Maketawa I bed-set

The Maketawa I bed-set (MkI) lies with sharp and parallel contact on top of ~10–15-cm-thick deposits of massive, poorly sorted and firm conglomerates (Fig. 3), which in southeastern locations consist of fine to coarse pebble gravels within a

clay-rich matrix. In other locations, the MkI rests with sharp contact upon ~5–10-cm-thick paleosols developed on top of other Members of the Manganui Formation.

The MkI includes four layers (Fig. 3) mainly exposed along southeastern and eastern flanks (Fig. 2). It is best seen at Curtis Ridge (Fig. 4) and Maketawa Hut sections (F and N, Figs. 1 and 2). Deposits of layers 2 and 3 are the most frequently exposed. Layer 2 comprises a normal-graded, well-sorted and clast-supported bed of yellow and crystalline pumice lapilli and dark-grey-lithic lapilli. Layer 3 comprises a characteristic set of pink and orange coloured, parallel-stratified, moderately sorted and occasionally pinching firm beds of pumice ash supporting aligned pumice and lithic lapilli and rare 1–5 cm-long charcoal twigs. Layers 2–3 are frequently deformed by blocks produced during deposition of the overriding lithic breccia of layer 4.

Layer 2 correlates with the Maketawa Tephra Formation mapped by Franks (1984) and dated at 2.9 ka B.P. by McGlone et al. (1988). Here, ^{14}C dating of charcoal within layers 3–4 at sections N and York track (Figs. 1 and 2) indicates an age of 2.2 cal ka B.P. for the MkI (Table 1), which is consistent with the ^{14}C age of 2.2 cal ka B.P. obtained by Turner (2008) for correlated deposits at section T (Fig. 1).

The Maketawa II bed-set

In most locations, the Maketawa II bed-set (MkII) lies with sharp contact over massive lithic breccias passing laterally into cross-stratified coarse lithic ash deposits (i.e. Grey PDC-I bed-set, Figs. 2 and 3). The latter are rarely separated with sharp contacts from a ~5–6-cm-thick paleosol developed on top of the MkI (Fig. 3). In a few sections, transitional contacts with weathered ash separate the MkII from the Grey PDC-I bed-set.

The MkII comprises five layers (Figs. 3 and 4) best seen at northeast locations (e.g. sections P–Q, Figs. 1 and 2). Although the MkII is traceable all along the eastern flanks of the volcano, its correlation is complex in proximal locations. Layers 1 and 4 consist of massive, moderately sorted, pinching beds of yellow pumice lapilli and dark-grey andesitic lithic lapilli supported by a matrix of pumice ash. Layers 2 and 5 comprise massive or reverse-graded, well-sorted and clast-supported beds of poorly vesicular and crystalline yellow pumice and andesitic lithic lapilli. Layer 3 comprises cross-stratified and massive, poorly to moderately sorted pinching beds of grey-lithic ash supporting imbricated lithic and pumice lapilli, interstratified with massive, clast-supported lenses of yellow pumice lapilli (Figs. 3 and 4).

In rare exposures (e.g. section P, Figs. 1 and 2), layer 3 thins to ~2–5 cm and becomes a distinctive grey, lithic-rich bed that contrasts with the bracketing yellow-white pumice deposits (Fig. 4). In addition, layer 2 and the pumice-rich lenses of layer 3 merge and expand to form a single, stratified, clast-supported and up to 75–80-cm-thick pumice-rich bed (Fig. 4). Layer 4 thickens to ~25 cm. Frequent, sharp-erosive angular contacts between layer 4 and several overriding lithic breccias occur where layer 5 has been completely eroded. These rapid transitions occur along sections spaced at ~50 m apart near the North Summit Track (e.g. sections P–Q and S, Figs. 1 and 2).

In several locations (e.g. section M; Figs. 1 and 2), the MkII is bracketed between deposits ^{14}C dated at 1.9 and 1.6 cal ka B.P. by Turner (2008; Table 1). This is consistent with the age of 1.8 cal ka B.P. of the underlying GI bed-set (e.g. section H; Figs. 1 and 2) calibrated from Neall and Alloway (1986).

The Maero Formation

The Maero Formation lies above the 3rd-order unconformity, and comprises deposits of the last ~850 years of volcanic activity of Mt. Taranaki (Druce 1966; Neall 1972, 1979; Neall et al. 1986; Cronin et al. 2003; Platz et al. 2012), represented by a minimum of 19 Members (Platz 2007). The most prominent deposits from oldest to youngest correspond to Members Te Popo Breccia and Te Popo Ash, Waingongoro Ash, Newall Ash, Waiweranui Ash, Puniho Ash and Burrell Lapilli. The most recent deposits of the Maero Formation correspond to three different post-AD 1755 Members (Platz 2007).

Based on the identification and correlation of the basal 3rd-order unconformity, the Maero Formation was here redefined to comprise a total of 23 Members, which includes older >1.0 ka deposits of Members Grey PDC-II, MrP-I, Kaupokonui and Grey PDC-III (Fig. 3). The Kaupokonui Member correlates with the ~1.2-cal ka B.P. Kaupokonui Tephra mapped by Whitehead (1976) and calibrated from Neall and Jansen (1984). ^{14}C dating of charcoal within deposits of the Grey PDC-III indicates an age of 1.0 cal ka B.P. (calibrated from Turner 2008).

The Te Popo Member (Tp) contains some of the thickest deposits of the Maero Formation, representing the Te Popo Episode recorded by Platz (2007). These deposits lie with sharp contacts on top of 10–15-cm-thick paleosols developed over Members Grey PDC-III or Kaupokonui (Fig. 3) or above of up to 100-cm-thick weathered ash deposits (section Q, Fig. 2). Paleosols and massive coarse-fine-ash deposits of the Newall, Waiweranui, Puniho and Burrell Lapilli Members overlie the Tp in few sections (Figs. 2 and 3).

The Tp comprises six layers exposed mainly on the northeastern volcano flanks (Figs. 3 and 4) and best preserved at the Veronica Slip and North Summit Track sections (U and Q, Figs. 1 and 2). Layers 2, 4 and 6 consist of mostly massive, well- and very well-sorted, clast-supported beds, composed of crystalline pumice lapilli and grey, bluish and altered-red dense or poorly vesicular porphyritic lithic lapilli (Fig. 3). These layers are interbedded with massive or parallel-stratified, poorly to well-sorted, matrix-supported deposits of layers

1 and 3 (Figs. 3 and 4). Layer 3 consists of three beds of lithic and pumice lapilli, at times reverse- or normal-graded (i.e. 3a to 3c; Figs. 3 and 4). Beds 3a and 3c are firm and the matrix includes a large fraction of white pumice ash, similar to the massive ash of layer 5. Bed 3b is clast rich but contains interstitial ash matrix.

Deposits of layer 1 (Figs. 3 and 4) correlate with westward-distributed 0.7-cal ka B.P. BAF deposits (^{14}C age calibrated from Cronin et al. 2003) of the Te Popo Breccia (Platz 2007), consistent with the ages of underlying 1.2–1.0 cal ka B.P. deposits at northeastern locations. The Te Popo Member encompasses both the Te Popo Breccia and likely the Te Popo Ash Members of Platz (2007).

The Fanthams Peak Lithosome

The Manganui Formation

At least four Members of the Manganui Formation, sourced at Fanthams Peak, were earlier mapped as the 'Manganui Tephra Formation' along the eastern area of Mt. Taranaki, up to ~20–25 km from the summit crater (Whitehead 1976; Alloway et al. 1995). In this work, the Manganui Formation encompasses a series of seven Members (Manganui A (MA) to Manganui G (MG), Fig. 3) with a characteristically basaltic composition (average 50.6 wt.% SiO_2; Price et al. 1992; Stewart et al. 1996; May 2003; Turner et al. 2011b) which contrasts with the typical average 57 wt.% SiO_2 for bed-sets above and below (Neall et al. 1986; Price et al. 1992; Stewart et al. 1996; Turner et al. 2011b; Platz et al. 2007, 2012) and sourced from the summit vent of Mt. Taranaki. The basal contact of the Manganui Formation is a sharp surface between a ~10-cm-thick paleosol developed on top of the 3.0 cal ka B.P. IgP-II bed-set and the lowermost Manganui A Member (Fig. 3; Table 1). The top of the Formation corresponds to a sharp, conformable contact between the uppermost <1.6 cal ka B.P. Manganui G Member and the Taranaki-sourced Curtis Ridge bed-set (cf. Turner et al. 2008b), both underlying the 3rd-order unconformity (Figs. 2 and 3).

Members Manganui A to D correlate with Manganui tephra beds a–d of Alloway et al. (1995). The Manganui G Member was previously included by Turner et al. (2008b) as part of the 'Curtis Ridge Lapilli' (CR Unit-1, Fig. 3), but at that time, Members Manganui E and F had not been identified. In southern flanks, Members Manganui B, C and D are interdigitated with at least three bed-sets sourced at Mt. Taranaki and consisting of pinching beds of light-grey andesitic lithic ash (i.e. MkP-I, MkP-II and MkP-III, Fig. 3) that pass laterally into lithic breccias. Similarly, Members Manganui E, F and G are intercalated with deposits of other six Mt. Taranaki-sourced bed-sets (e.g. Maketawa I, Maketawa II and Curtis Ridge; Fig. 3).

Alloway et al. (1995) dated Members Manganui A to D between 3.3 and 2.9 ka B.P. Here, ^{14}C dating of charcoal within deposits of bed-sets IgP-II and Maketawa I (e.g. section N, Figs. 1 and 2) bracket Members Manganui A to E between 3.0 and 2.2 cal ka B.P. (Table 1). ^{14}C dating of a log within lithic breccias of bed-sets MkP-I and -II (section B, Figs. 1 and 2) indicates that Members Manganui A and B are >2.6 cal ka B.P. in age (Table 1). ^{14}C dating of charcoal within deposits of the encapsulating bed-sets Maketawa II and Grey PDC-III (section M, Figs. 1 and 2) indicate that Members Manganui F and G are <1.6 to >1.0 cal ka B.P. (calibrated from Turner 2008).

The Manganui A Member (MA) comprises at least three layers (Fig. 3) resting with a sharp lower contact above ~6-cm-thick paleosols and up to 10-cm-thick weathered ash, best seen at Curtis Ridge and Veronica track sections (F and R, Fig. 1). Layers 1–2 are reverse to normally graded, very well-sorted, clast-supported and often firm deposits of crystal-rich, dark-brown pumice and dark-grey scoria lapilli and ash. Layer 3 consists of distinctive parallel- and cross-stratified, moderately sorted and pinching-swelling beds of dark bluish-grey-lithic ash (Fig. 3). The MA contains the most vesicular pyroclasts of the Manganui Formation.

The Manganui B Member (MB) lies above ~5–6-cm-thick edafized and firm deposits of fine-sand capping the MA (Fig. 3). The MB comprises a very distinctive reverse-graded and occasionally massive, moderately to well-sorted, clast-supported and rarely matrix-supported bed of heterogeneous lithic lapilli, rich in cauliflower and bread-crust bombs. The Manganui C Member (MC) is separated from the underlying MB by bed-sets MkP-I and MkP-II (Fig. 3), ~5-cm-thick edafized ash deposits and occasional firm deposits of coarse sand. The MC is made up of very friable, reverse to normal-graded, well- to very well-sorted and clast-supported thin beds of moderately crystalline dark-grey-lithic lapilli, dark-brown pumice and black scoria lapilli and ash.

The Manganui D Member (MD) contains the thickest deposits of the Manganui Formation (Fig. 3). The MD rests with sharp contact on top of edafized firm deposits of coarse sand, rich in dark juvenile clasts from the underlying Manganui Members. These same types of sand deposits are also interstratified with basal beds of the MD (Fig. 3).

The MD comprises at least three pyroclastic layers, exposed in most sections (Fig. 2), and a lava flow (layer 2b, Fig. 4). Layers 1 and 2 comprise reverse to normal-graded, well- and very well-sorted and clast-supported beds, made up of dense dark lithic lapilli and moderately crystalline pumice and scoria lapilli and ash. Violet-red and orange-altered lithics are common in layer 1 but rare in layer 2. Layer 3 is a very distinctive deposit of four reverse to normal-graded, well-sorted and clast-supported lapilli beds (Fig. 3) made up of juvenile clasts similar to layers 1–2 but with higher altered and accidental lithic concentrations in middle beds (i.e.

orange, red and white-bleached altered angular lithics; and black-grey dioritic accidentals).

With distance, layer 3 passes into a single stratified deposit of evenly mixed juveniles and altered and accidental lithics. In eastern and southeastern locations, layer 3 is partially or fully replaced by firm sand deposits rich in juvenile clasts from the MD (Figs. 3 and 4); whereas in few southeastern sections (e.g. sections C and D; Figs. 1 and 2), layers 1–3 are capped and partially or fully eroded by lava flows sourced at Fanthams Peak (Fig. 4).

The Manganui E Member (ME) is found in only few locations (e.g. sections N and R, Figs. 1 and 3), lies above ~2–6-cm-thick paleosols developed on top of lapilli-rich breccias and is often partially eroded or fully replaced by overriding breccias rich in ME-lapilli. The ME consists of reverse to normally graded, well- and very well-sorted and clast-supported beds of poorly vesicular, dark-grey-lithic lapilli, scoria lapilli and brown pumice lapilli. Orange-reddish scoriaceous fragments give ME a distinctive appearance compared with earlier Manganui Members.

The Manganui F Member (MF) comprises a rarely preserved deposit exposed in northeastern locations (e.g. section Q, Figs. 2 and 4). The MF rests with a gradational contact upon weathered massive fine-ash deposits, and consists of reverse to normally graded, well-sorted and clast-supported beds of moderately crystalline, dark-brown and grey lithics, pumice and scoria lapilli, and the Member's most distinctive poorly vesicular, scarlet-red lithic lapilli (Figs. 3 and 4).

Interpretation of deposits and associated volcanic hazard

The lithofacies associations of the different bed-sets that comprise the late-Holocene Members deposited on Mt. Taranaki (Fig. 3) allow them to be classified within three categories: (a) fall deposits from a sustained, convective eruption column (cf. Cioni et al. 2000, 2008; Arce et al. 2003, 2005; Pardo et al. 2012a, b); (b) PDC deposits, including column-collapse and dome-collapse sourced currents (cf. Brown and Branney 2004; Lube et al. 2011; Cronin et al. 2013; Kim et al. 2014); and (c) lahar deposits from syn- and post-eruptive debris flows and hyperconcentrated flows.

Pyroclastic fall deposits

The diagnostic features of fall deposits in the proximal areas are mantling of paleotopography, even thickness, good-sorting (according to 1st-order visual classes of Cas et al. 2008) and clast-supported framework. Beds range from massive to graded (both reverse and normal) and/or have 'shower-bedded' stratification, reflecting vertical grain-size or compositional changes. The deposits are generally friable and dominated by pumice clasts, which are normally lapilli-grade with local blocks and bombs (the latter being mainly ballistically emplaced).

Single fallout units are up to 2 m thick, such as from the Kokowai and Te Popo eruptions (Fig. 5). Fallout-generated deposits are associated with 28 of the 53 eruptions and 45% of the total thickness of the studied pyroclastic succession. Around 57% of the fall deposits are widespread, significantly coarse grained and thick enough to be representative of the maximum eruption column heights produced at Mt. Taranaki over the Holocene (cf. ~14-km-height column of the AD 1655 Burrell eruption, Platz et al. 2007).

Pyroclastic debris dispersed by clouds or plumes is an expected hazard from large eruptions at andesitic volcanoes. Ash has impacts in the air (including air-transport routes), on land (agriculture), and in water environments and may severely damage infrastructure due to its abrasive, corrosive, acidic and conductive properties (Cronin et al. 1998, 2003; Wilson et al. 2011). Ash from Mt. Taranaki plumes was distributed dominantly across the northeastern and east-southeastern flanks (Fig. 2) due to New Zealand's North Island's prevailing winds, covering currently populated areas of ~1600 km^2 (Neall 1972; Topping 1972; Whitehead 1976; Alloway et al. 1995). Distal fall deposits from Mt. Taranaki have also been identified in maar-crater sediments in Auckland, 280 km away from the volcano (Shane 2005).

Pyroclastic density currents

PDC units in Mt. Taranaki include both pumice and lithic-rich proximal deposits, with a common pinching and pinching-and-swelling geometry, which drape ridges and thicken in paleovalleys. The diagnostic features of PDC deposits are their generally poor sorting and matrix support; they vary from massive to parallel- and cross-stratified and contain a mixture of ash, lapilli and blocks, with common charcoal fragments.

The stratigraphic succession suggests that PDCs were the most frequent proximal volcano-sedimentary process during Holocene Mt. Taranaki eruptions, generating deposits during 38 of the 53 eruption events/episodes studied, and producing 55 vol.% of the total composite pyroclastic deposit thickness (Fig. 5). PDC units can be up to 2 m thick on ridges, and much thicker in valleys. In this proximal area, the PDC deposits may constitute up to ~80 vol.% of the record of an eruption episode (e.g. Upper Inglewood and Korito eruptions; Fig. 5), and could be deposited both by one-off flows, or from a sequence of events (e.g. Grey PDC-I and -II eruptions, Fig. 3). PDC units almost universally accompanied eruptions that produced thick fall deposits during complex eruption episodes (e.g. Kokowai eruption, Fig. 3).

Pumice-dominated PDC deposits, commonly associated with pumice-rich fall deposits, are interpreted as resulting from column collapse under open-conduit conditions. In

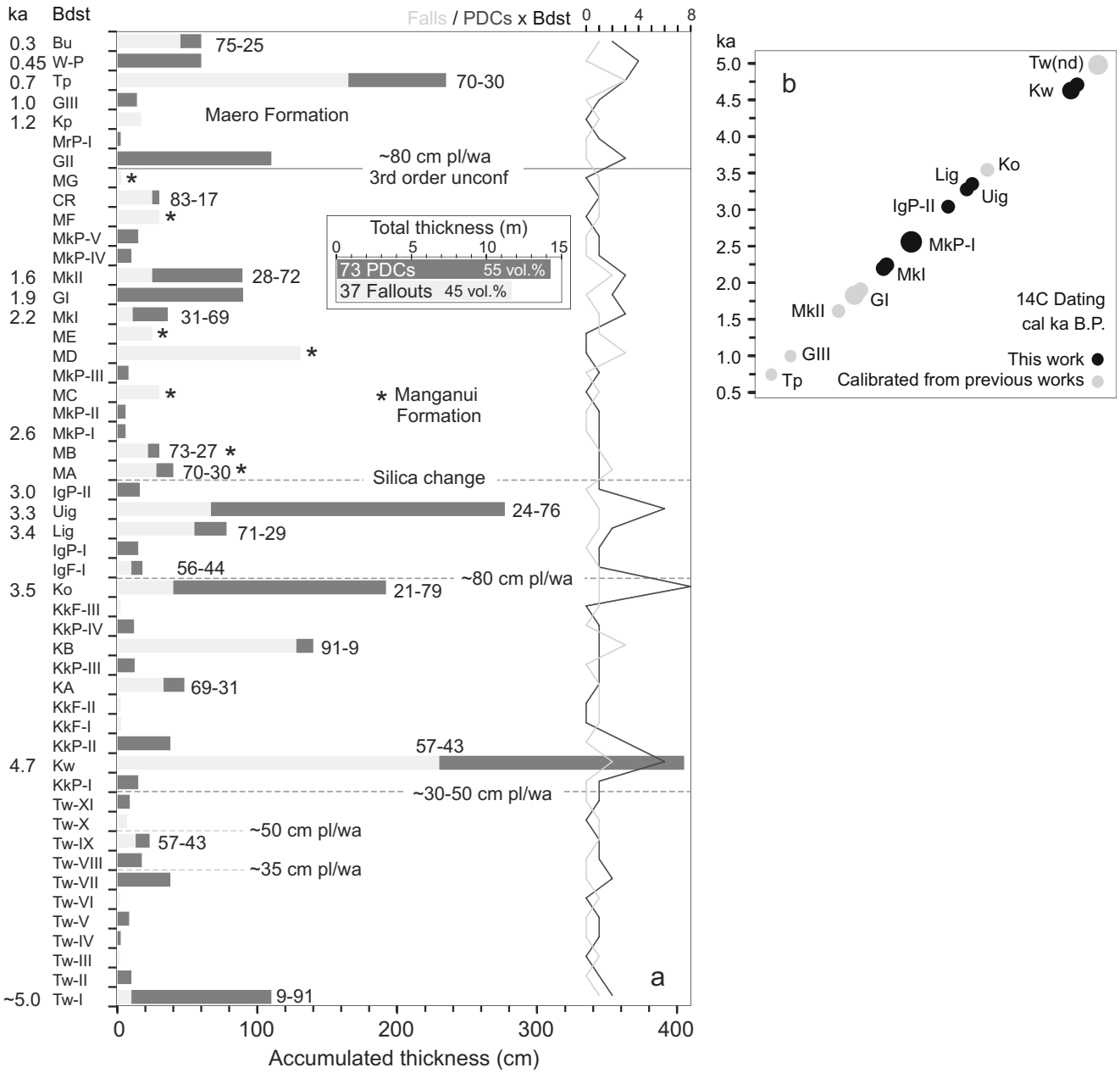

Fig. 5 **a** Total accumulated thickness of fall and pyroclastic density current (*PDC*) deposits per bed-set (*Bdst*) in centimetres, and total thickness per pyroclastic deposit type in metres (see *inset*). *Numbers accompanying bars* (e.g. 71–29) indicate volume percentages of fall-PDC deposits. The *line diagram* indicates number of layers of fall and PDC deposits (units) per bed-set. *Unconf* unconformity, *pl/wa* intervening paleosol and/or weathered ash deposits in centimetres thick. Refer to text and Fig. 3 for bed-set abbreviations. **b** Calibrated ^{14}C ages from this work and previous works. The size of each *circle* is proportional with the corresponding dating error (see Table 1 for complete data and references)

contrast, lithic-dominated PDC deposits are interpreted as resulting from lava-dome collapse, under initially closed-conduit conditions. The massive to stratified lithofacies is attributed to concentrated to dilute PDCs, respectively. Both types of PDCs have been observed in recent historical eruptions of similar composition, type and scale (e.g. Saucedo et al. 2010; Lube et al. 2011; Cronin et al. 2013).

The run-out of PDCs is commonly influenced by their volumes. Previous studies indicated that low-volume PDCs at Mt. Taranaki commonly reached 10–15 km from the crater (Procter et al. 2010; Platz et al. 2007, 2012). However, longer run outs could be expected during extended eruption episodes, because deep valleys become in-filled and smoothed by earlier deposits (e.g. Lube et al. 2011; Cronin et al. 2013).

Field evidence for the distribution of PDC deposits of Mt. Taranaki from multiple past studies suggests that any of the volcanic flanks could be impacted, with arguably the northwestern sector being at present most susceptible due to the collapsed northwestern crater margin (Procter et al. 2010; Platz et al. 2007, 2012). During future eruptions, PDCs would pose a very high threat to all the forested areas of the Egmont National Park and the adjacent inhabited farmland (Figs. 1 and 2). Given the high abundance of PDC units within the deposits studied, it must be assumed by hazard managers that almost every eruption of Mt. Taranaki will produce at least one PDC of some type.

Revised eruption history

Comparison with previous work

The example of Fig. 3a demonstrates that the volcanic processes during the <5-ka eruption events and episodes at this volcano are far more complex than those interpreted from previous ring-plain and distal deposits. Previous studies of ring-plain deposits at Mt. Taranaki estimated 27 tephra beds within 12 Tephra Formations (cf. Neall 1972; Franks 1984; Alloway et al. 1995). However, according to the International Stratigraphic Code (Salvador 1994), genetic terms should be avoided when naming lithostratigraphic units. In addition, the significance of each lithostratigraphic unit defined in previous works, in terms of eruption activity and source, remains unclear. Each of the defined 'Tephra Formations' could either be (a) deposits produced by only one fallout/PDC during a single eruption event (e.g. The Kaupokonui Member), (b) deposits produced by one or more fall/PDCs within a multiple-eruption episode (e.g. The Maketawa I bed-set) or (c) deposits produced during several different eruption events or episodes (e.g. The Manganui Formation). In this respect, some of the 'Formations' defined might provide information about layers (e.g. a flow), but do not contain details about distinct eruption events/episodes. Furthermore, using Tephra Formations to define volcanic units excludes any potential syn-eruptive lithofacies variation with distance, from a proximal pyroclastic deposit to a distal volcaniclastic and/or epiclastic deposit (e.g. syn-eruptive lahars).

In the present study, we therefore propose abandonment of the previously defined Tephra Formations, as has been done in schemes earlier applied by Cronin et al. (2003) and Platz (2007) to redefine the uppermost Maero Formation following the international rules for the definition of lithostratigraphic units. There is only one more Formation that is mappable, distinctive in the field and with clear basal-and-top contacts, which is the Manganui Formation. For the rest of the stratigraphy, we redefined units bounded by erosive surfaces or paleosols, suggesting time breaks in eruptive activity, as bed-sets.

We estimated a total of 37 pyroclastic fall deposits and 73 individual PDC units formed during 53 different eruptions (events or episodes), in the period between 5 and 0.3 cal ka B.P. (Fig. 5). Previous studies recognized only ten fall deposits as being related to PDCs (Turner et al. 2008b; Platz et al. 2007, 2012). This poor representation of PDC deposits in ring-plain areas was also noted in high-resolution distal swamp- and lake-core sediment pyroclastic fallout records surrounding Mt. Taranaki (Turner et al. 2008b, 2009, 2011a).

Despite the improved resolution obtained in the present research, the new proximal record still does not represent all eruptions with deposits known from distal swamp- and lake-core sediment records over the same time period (e.g. up to 62 in Green et al. 2016).

Late-Holocene eruptions of Mt. Taranaki

For simplicity, we have organized the 53 late-Holocene eruptions, sourced from the summit of Mt. Taranaki and Fanthams Peak, according to peaks in pyroclastic and epiclastic (in this case only for sediments clearly produced from post-eruptive pyroclast-remobilization during inferred periods of volcanic quiescence; Fisher and Schmincke 1984) bed-set deposition and soil formation, interpreted from maximum deposit thickness through time (Fig. 5). Similarly, the peaks in pyroclastic deposition associated with the largest eruption episodes during the last 5 ka, were compared with the maximum thickness produced by the 3.2×10^8 m^3 fall deposits generated by a ~14-km-high column during the eruption of the sub-Plinian Burrell episode (Bu; Platz et al. 2007; Fig. 5).

At least 11 different eruption events/episodes, separated by periods of quiescence of different length, occurred between ~5 and 4.7 cal ka B.P. (Fig. 5), producing five pyroclastic fall deposits and ten PDC units localized down the north and northeast volcano flanks (Fig. 2). The largest eruption during this period (Tw-I bed-set, Fig. 3) began with BAFs in-filling the Kokowai Stream valley, which was followed by a short-lived eruption column that produced pumice-rich deposits. Subsequent events produced sequences of hot column-collapse PDCs from brief, short-lived eruption columns, similar or smaller than the Tw-I eruption based on the thinner deposits generated (Fig. 5).

Following a period of quiescence, the largest late-Holocene eruption episode of Mt. Taranaki produced the thickest deposits of the 4.7–4.6-cal ka B.P. Kokowai bed-set (Figs. 3 and 5). The Kokowai eruption started with BAFs in-filling the southeastern valleys of the Kaupokonui Stream. Two eruption columns accompanied by column-collapse PDCs produced thick and widespread fall deposits blanketing the north and east Taranaki Peninsula.

Subsequently, ten eruptions produced eight fallouts and 16 PDCs between 4.7 and 3.5 cal ka B.P., many of which produced only ~5–15-cm-thick deposits (Fig. 5). The Kapuni B

episode produced a particularly thick, southeast-dispersed fallout succession, without any large PDC deposits (Fig. 5). The Korito bed-set was deposited from the last large eruption episode during this time period; but, in contrast to the others, it was dominated by production of a succession of column-collapse PDCs (Fig. 5) with minor fall units (Fig. 3).

The next major eruptions occurred after a period during which up to 80-cm-thick weathered fine ash accumulated at many sites, either due to very small eruptions or by wind-remobilised ash. Five eruption episodes produced three fall-outs and ten PDCs between 3.4 and 3.3 cal ka B.P. (Fig. 5). The earliest, Lower Inglewood eruption produced pumice-rich PDC and fall deposits similar in thickness to the sub-Plinian Burrell eruption (Platz et al. 2007; Figs. 3 and 5). Following a brief interval of quiescence, the Upper Inglewood eruption produced the thickest PDC succession in the late-Holocene history of Mt. Taranaki, having northeast-dispersed pumice fallout (Figs. 3 and 5).

A brief quiescence, during which ~20 cm thick of weathered massive fine-ash accumulated, preceded a sudden shift to paired eruption of basaltic (average 50.6 wt.% SiO_2) and andesitic (average 57 wt.% SiO_2) variants (Price et al. 1992; Stewart et al. 1996; May 2003; Turner et al. 2011b) from two centres, the parasitic Fanthams Peak (1952 m-elevation) and the summit crater (2518 m), respectively. From these two centres, 17 eruptions occurred between ~3 and 1.5 cal ka B.P., producing 14 fall and 17 PDC units (Fig. 5). Seven of these eruptions were sourced at Fantham's Peak and produced eight fallouts and two PDC units that deposited seven bed-sets (i.e. The Manganui Formation) encompassing ten layers formed by distinctive basaltic, dark-grey and black lithics, dark-grey scoria (i.e. approximately dense clasts of thick-walled vesicles) and brown pumice (i.e. approximately fragile clasts of thin-walled vesicles). The other ten eruptions deposited 19 layers of andesitic pumice and lithic compositions, corresponding with four fallouts and 15 PDC units (Fig. 5).

The contrast between fall-dominated eruptions of basaltic composition and prevalent PDCs from the andesitic eruptions of this period (Fig. 3) is noteworthy, and potentially reflects differing conduit conditions, magma supply rates and volatile contents; this needs to be further investigated. Preliminarily, the key feature of the summit crater appears to be choked conduits, with crystalline mush within the conduit and/or capping lava domes (cf. Platz et al. 2007, 2012 and data presented above). This means that eruption events/episodes are more complex, involving a range of BAFs, vulcanian blasts with unstable columns producing further column-collapse PDCs and eventually sustained columns, only when the conduit has been cleared. By contrast, the Fanthams Peak eruptions appear to be characterized by more open-vent conditions, producing fall deposits from stable eruption columns. Occasional lava flows interspersed within the eruption sequence (e.g. Manganui D bed-set; Figs. 2 and 4) and the basaltic and less crystalline composition of the Fantham's eruptive products suggest lower viscosity magmas and rapid transit through the upper conduit system. Some of the most mafic eruptions of the period were also located from subsidiary vents just below and north of the Fanthams Peak area, in the Rangitoto flat (noted by Turner et al. 2008a, b).

Despite the basaltic compositions (Price et al. 1992; Stewart et al. 1996; May 2003; Turner et al. 2011b), the largest eruption of the Fanthams Peak area produced the east and northeast-dispersed Manganui D fall succession (Figs. 2 and 3), which is similar in thickness to the fall deposits of the Kapuni B bed-set, and thicker than the 3.2×10^8 m^3 fall deposits produced by the ~14-km-high column of the sub-Plinian Burrell eruption (Platz et al. 2007; Fig. 5). Many of other Mt. Taranaki's summit eruptions, contemporaneous with the activity of Fanthams Peak, generated thick BAFs and column-collapse PDCs but comparatively thin pumice fall deposits (e.g. Maketawa I and II bed-sets; Figs. 3 and 5).

Most deposits of the Manganui Formation appear similar to the deposits produced during the eruptions of monogenetic basaltic volcanoes (e.g. Rowland et al. 2009) but, in contrast, the former span ~1500 years and so are much longer than the eruption of a single monogenetic volcano. In addition, the relatively thin (~1–6 cm) paleosols and weathered massive fine-ash deposits that separate some of the Manganui Members (e.g. MA-MB, MB-MC and MD-ME; Fig. 3) represent longer intervals of quiescence than were observed during, e.g. the 10–15 years eruption episodes of Paricutin and Jorullo (Rowland et al. 2009), even if we assume that other intervening pyroclastic and volcaniclastic deposits were produced by syn-eruptive units, e.g. BAFs and lahars.

First-order estimates considering segments of 120- and 250-cm-thick pyroclastic, epiclastic and paleosol deposits bracketing 3.0–2.6 and 2.6–2.2 cal ka B.P., respectively, and comprising Members MA-ME (Fig. 3), suggest the accumulation of 1 cm of soil or weathered massive ash in 16 to 27 years. In this hypothetic rapid soil-forming environment of Mt. Taranaki, and considering ^{14}C dating errors of maximum 100 years (Table 1), Members MA-ME were likely deposited during a single yet very long ~190–320 years episode at ~2.6 ka, separated by quiescence intervals of ~400 years from deposition of the under- and overlying bed-sets (i.e. from ~3–2.6 and ~2.6–2.2 ka, respectively, Fig. 3). By contrast, Members MF-MG rest on top of Taranaki-sourced deposits of <1.6 cal ka B.P., suggesting that at least 600–1000 years separate the youngest from the oldest Manganui Members.

By this means, the Manganui Formation was produced from relatively frequent and multi-episodic eruptions. Fanthams Peak must be considered a potential future eruptive vent together with the summit crater of Mt. Taranaki, able to produce large-volume basaltic eruption episodes (cf. Coltelli et al. 1998) as have other multi-vent

basaltic to andesitic volcanoes (e.g. Tongariro Volcanic Complex, Nairn et al. 1998).

The stratigraphic sequence indicates that Fantham's vent became quiescent at ~1.6–1.4 ka, but the Summit vent remained active, producing at least nine <1.5 ka eruptions that generated five fall deposits and at least 14 PDC units (Fig. 5). Some of the eruptions produced thick fall deposits that correspond to the 1.2 cal ka B.P. Kaupokonui Member (calibrated from Neall and Jansen 1984) and the ~AD 1655 Burrell Lapilli (Druce 1966; Topping, 1971; Platz et al. 2007). Also, many eruptions of this period produced thin fine-ash layers on the proximal eastern volcanic flanks, but emplaced valley-filling BAF layers on the northwestern flanks (Druce 1966; Neall 1972; Platz 2007; Platz et al. 2012).

The thickest deposit, suggesting the largest eruption of the last ~1000 years at Mt. Taranaki, corresponds to the ~0.7-cal ka B.P. Te Popo Member, involving three fallouts and three PDC units that formed deposit sequences distributed to the northeast and west (Fig. 3). The episode started with the emplacement of hot BAFs within the western valleys of the volcano (Platz et al. 2012), with correlative ash blankets on the northeastern side (Fig. 2). The following three eruption columns covered the east of Mt. Taranaki under ash and pumice fall, with one collapsing to produce a PDC. The eruption column(s) generated fall deposits intermediate in thickness between those of the Burrell and the Kokowai bed-sets (Figs. 3 and 5).

Within this context, it remains clear that proximal data are essential for increasing the precision of eruptive frequency records. Where these are missing, tephrochronological and hazard-related studies should specify and document the limitations of their interpretations based on incomplete datasets. Statistical models accounting for missing proximal data need to be established in order to assess eruption frequencies and repose-time periods.

Interpretations based only on intermediate-to-distal records could also oversimplify the eruption dynamics, particularly when short run-out depositional events are not represented in medial or distal sites. Hence, we suggest conservative documentation when reporting, for example, sustained eruption columns based on intermediate-to-distal tephra records could be miss-inferred when the proximal PDC deposits are not included.

Conclusions

A detailed new stratigraphy of proximal volcanic deposits on Mt. Taranaki provides stratigraphical and volcanological data for analysis of 53 eruption events and episodes in the period from ~5 to 0.3 ka. The proximal deposits record nine fewer eruptions than does the highest-resolution compilation of medial fall deposits in swamp and lake sequences (Green et al. 2016), but the proximal record gives greater detail about eruption processes (e.g. Fig. 3a). This additional information is particularly important for developing an understanding of the volcanic hazards, including the style and sequence of events, as well as realistic eruption scenarios for hazard management planning.

From these new proximal details it is clear that pyroclastic density currents (block-and-ash flows and column-collapse PDCs) are the most common hazards at Mt. Taranaki, in spite of the fact that they have been poorly recognized from past studies. Furthermore, it is clear that many eruptions are complex, with multiple phases, including dome growth and collapse, and the repeated production of eruption columns which often collapse (e.g. Fig. 3a). The new data also shows the great diversity of eruptive styles of largest eruption episodes. We infer tentatively that diversity might be controlled by magma composition and conduit conditions (e.g. Kokowai versus Upper Inglewood versus Manganui D eruptions; Fig .3). In the period between ~3 and 1.5 cal ka B.P., two vents were erupting and displayed a contrast in composition and eruptive style. Fanthams peak produced basaltic magmas with steady eruptive columns and dominantly fallouts, while the andesitic summit vent produced many domes, short-lived dense vulcanian eruption columns and dominantly PDCs. The hazard profiles of these two, potentially simultaneous eruption sources must be carefully considered in future hazard studies.

In addition, we have revised fall deposit correlations drawn between northeast-distributed and east to southeast-distributed fallout lobes of apparently similar relative stratigraphic position surrounding Mt. Taranaki. At this and other similar volcanoes around the world, medial soil stratigraphies without precise chronology do not provide ideal conditions to relate similar-appearing fall deposits at different sectors around a volcano. By showing more precisely breaks between eruption events/episodes and the strong-sector based variations in stratigraphy, proximal studies can provide a more realistic number of eruptions and a more reliable expectation for eruptions. It remains to be seen whether the large pre-5 ka B.P. tephras in the Taranaki record, which are also depicted with a bilobate form (e.g. Alloway et al. 1995), represent single or multiple-eruption events or episodes.

This work shows the importance of recording, where possible, detailed lithostratigraphic data for the nearest-vent sites possible on stratovolcanoes. This approach provides unique insights into the eruptive record. Not only are some eruptions newly recorded but also the depth of understanding about the diversity and style of eruption processes can be evaluated, along with the range of eruption sequences that may help develop realistic scenarios for emergency managers.

Acknowledgements We thank G. Kereszturi, G. Gomez and E. Sandoval for their support in the field; M. Damaschke and V. Neall for

discussion and comments; and K. Arentsen for assistance with logistics. Constructive comments of Lucia Capra, two anonymous reviewers and James White improved this article. We thank the Department of Conservation in Taranaki for their support with permits. SJC is supported by the 'Quantifying exposure to specific and multiple volcanic hazards' programme of the NZ Natural Hazards Research Platform. RTO is supported by a Massey University Doctoral Scholarship, a CONACyT (Mexico) Doctoral Scholarship and the George Mason Trust of Taranaki.

References

Alberico I, Petrosino P, Lirer L (2011) Volcanic hazard and risk assessment in a multi-source volcanic area: the example of Napoli city (southern Italy). Nat Hazards Earth Syst Sci 11:1057–1070

Alloway B, Lowe DJ, Chan RPK et al (1994) Stratigraphy and chronology of the stent tephra, a c. 4000 year old distal silicic tephra from Taupo volcanic Centre, New Zealand. NZ J Geol Geoph 37:37–47

Alloway B, Neall VE, Vucetich CG (1995) Late quaternary (post 28, 000 year B.P.) tephrostratigraphy of northeast and Central Taranaki, New Zealand. J Royal Soc NZ 25:385–458

Alloway B, McComb P, Neall V et al (2005) Stratigraphy, age, and correlation of voluminous debris-avalanche events from an ancestral Egmont volcano: implications for coastal plain construction and regional hazard assessment. J Royal Soc NZ 35:229–267

Andreastuti SD, Alloway BV, Smith IEM (2000) A detailed tephrostratigraphic framework at Merapi Volcano, Central Java, Indonesia: implications for eruption predictions and hazard assessment. J Volcanol Geoth Res 100:51–67

Arce JL, Macias JL, Vazquez-Selem L (2003) The 10.5 ka Plinian eruption of Nevado de Toluca Volcano, Mexico: stratigraphy and hazard implications. Geol Soc Am Bull 115:230–248

Arce JL, Cervantes KE, Macias JL, Mora JC (2005) The 12.1 ka Middle Toluca pumice: a dacitic Plinian–subPLINIAN eruption of Nevado de Toluca in Central Mexico. J Volcanol Geoth Res 147:125–143

Avellan DR, Macias JL, Sosa-Ceballos G, Velasquez G (2014) Stratigraphy, chemistry, and eruptive dynamics of the 12.4 ka Plinian eruption of Apoyeque volcano, Managua, Nicaragua. Bull Volcanol 76:792

Bourdier JL, Pratomo I, Thouret JC et al (1997) Observations, stratigraphy and eruptive processes of the 1990 eruption of Kelut volcano, Indonesia. J Volcanol Geoth Res 79:181–203

Bronk-Ramsey C (2009) Bayesian analysis of radiocarbon dates. Radiocarbon 51(1):337–360

Brown RJ, Branney MJ (2004) Event-stratigraphy of a caldera-forming ignimbrite eruption on Tenerife: the 273 ka Poris Formation. Bull Volcanol 66:392–416

Carn SA, Pallister JS, Lara L et al (2009) The unexpected awakening of Chaitén volcano, Chile. EOS Transactions, AGU 90(24):205–206

Cas R, Porritt L, Pittari A, Hayman P (2008) A new approach to kimberlite facies terminology using a revised general approach to the nomenclature of all volcanic rocks and deposits: descriptive to genetic. J Volcanol Geotherm Res 174:226–240

Cioni R, Marianelli P, Stantacroce R, Sbrana A (2000) Plinian and subPlinian eruptions. In: Sigurdsson H, Houghton BF, McNutt SR, Rymer H, Stix J (eds) Encyclopedia of volcanoes. Academic Press, San Diego, pp. 477–494

Cioni R, Bertagnini A, Santacroce R, Andronico D (2008) Explosive activity and eruption scenarios at Somma-Vesuvius (Italy): towards a new classification scheme. J Volcanol Geotherm Res 178:331–346

Coltelli M, Del Carlo P, Vezzoli L (1998) Discovery of a Plinian basaltic eruption of Roman age at Etna volcano, Italy. Geol 26(12):1095–1098

Cronin SJ, Hedley MJ, Neall VE, Smith G (1998) Agronomic impact of tephra fallout from 1995 and 1996 Ruapehu volcano eruptions, New Zealand. Environ Geol 34:21–30

Cronin SJ, Stewart RB, Neall VE et al (2003) The AD1040 to present Maero eruptive period of Egmont Volcano, Taranaki, New Zealand. Geol Soc NZ Misc Publ 116A:43

Cronin SJ, Lube G, Dayudi DS et al (2013) Insights into the October-November 2010 Gunung Merapi eruption (Central Java, Indonesia) from the stratigraphy, volume and characteristics of its pyroclastic deposits. J Volcanol Geoth Res 261:244–259

Downey WS, Kellett RJ, Smith IEM et al (1994) New palaeomagnetic evidence for the recent eruptive activity of Mt. Taranaki, New Zealand. J Volcanol Geoth Res 60:15–27

Druce AP (1966) Tree-ring dating of recent volcanic ash and lapilli, Mt Egmont. NZ J Botany 4:3–41

Espindola JM, Zamora-Camacho A, Godinez ML et al (2010) The 1793 eruption of San Martín Tuxtla volcano, Veracruz, Mexico. J Volcanol Geoth Res 197:188–208

Fisher R, Schmincke HU (1984) Pyroclastic rocks. Springer-Verlag, Berlin, p. 472

Franks AM (1984) Soils of Eltham County and the tephrochronology of central Taranaki. Dissertation, Massey University, Palmerston North, New Zealand

Green RM, Bebbington MS, Jones G et al (2016) Estimation of tephra volumes from sparse and incompletely observed deposit thicknesses. Bull Volcanol 78:25

Henrys S, Reyners M, Bibby H (2003) Exploring the plate boundary structure of North Island, New Zealand. EOS, Trans Am. Geophys Union 84:289–294

Hogg AG, Hua Q, Blackwell PG et al (2013) SHCAL13 southern hemisphere calibration, 0-50,000 years cal BP. Radiocarbon 55(4):1889–1903

Houghton BF, Wilson CJN, Del Carlo P et al (2004) The influence of conduit processes on changes in style of basaltic Plinian eruptions: Tarawera 1886 and Etna 122 BC. J Volcanol Geoth Res 137:1–14

Kim GB, Cronin SJ, Yoon WS, Sohn YK (2014) Post 19 ka B.P. eruptive history of Ulleung Island, Korea, inferred from an intra-caldera pyroclastic sequence. Bull Volcanol 76:802. doi:10.1007/s00445-014-0802-1

King PR, Thrasher GP (1996) Cretaceous-Cenozoic geology and petroleum systems of the Taranaki Basin, New Zealand. Institute of Geological and Nuclear Sciences Monograph 13

Lube G, Cronin SJ, Thouret JC, Surono (2011) Kinematic characteristics of pyroclastic density currents at Merapi and controls on their avulsion from natural and engineered channels. GSA Bull 123(5/6): 1127–1140

Lucchi F (2013) Stratigraphic methodology for the geological mapping of volcanic areas: insights from the Aeolian archipelago (southern Italy). Geological Society, London, Memoirs 37:35–53

Macias JL, Sheridan MF, Espindola JM (1997) Reappraisal of the 1982 eruptions of El Chichón Volcano, Chiapas, Mexico: new data from proximal deposits. Bull Volcanol 58:459–471

May DJ (2003) The correlation of recent tephra with lava flows on Egmont volcano, Taranaki, New Zealand using evidence of mineral chemistry. Dissertation, University of Auckland, Auckland, New Zealand

McGlone MS, Neall VE, Clarkson BD (1988) The effect of recent volcanic events and climate changes on the vegetation of Mt Taranaki (Egmont). New Zealand, N Z J Bot 26:123–144

Mortimer N, Tulloch AJ, Ireland TR (1997) Basement geology of Taranaki and Wanganui basins, New Zealand. NZ J Geol Geoph 40:223–236

Nairn IA, Kobayashi T, Nakagawa M (1998) The ~10 ka multiple vent pyroclastic eruption sequence at Tongariro volcanic Centre, Taupo volcanic zone, New Zealand: part 1. Eruptive processes during regional extension J Volcanol Geoth Res 86:19–44

Neall VE (1972) Tephrochronology and tephrostratigraphy of western Taranaki (N108-109), New Zealand. NZ J Geol Geoph 15:507–557

Neall VE (1979) Sheets P19, P20, and P21. New Plymouth, Egmont and Manaia. 1st ed. Geological map of New Zealand 1:50,000. 3 maps and notes. NZ Dept of Scientific and Industrial Res, Wellington

Neall VE (2003) The volcanic history of Taranaki. Institute of Natural Resources, Massey University, Soil & Earth Sciences Occasional Publication 2

Neall VE, Alloway BV (1986) Quaternary volcaniclastics and volcanic hazards of Taranaki. NZ Geol Surv Rec 12:101–137

Neall VE, Alloway BV (2004) Quaternary geological map of Taranaki. Institute of Natural Resources-Massey University, Soil and Earth Sciences Occasional Publication No. 4

Neall VE, Jansen HS (1984) Anomalous radiocarbon dates from Mt. Egmont. Geol Soc of NZ, Miscellaneous Publication 31A.

Neall VE, Stewart RB, Smith IEM (1986) History and petrology of the Taranaki volcanoes. In: Smith IEM (ed) Late Cenozoic volcanism. Royal Society of New Zealand Bulletin 23:251–263

Pardo N, Cronin SJ, Palmer A, Németh K (2012a) Reconstructing the largest explosive eruptions of Mt. Ruapehu, New Zealand: lithostratigraphic tools to understand subPlinian-Plinian eruptions at andesitic volcanoes. Bull Volcanol 74:617–640

Pardo N, Cronin SJ, Palmer A et al (2012b) Andesitic Plinian eruptions at Mt. Ruapehu: quantifying the uppermost limits of eruptive parameters. Bull Volcanol 74:1161–1185

Platz T (2007) Aspects of dome-forming eruptions from Andesitic Volcanoes exemplified through the Maero Eruptive Period (1000 yrs B.P. to Present) activity at Mt. Taranaki, New Zealand. Dissertation, Massey University, Palmerston North, New Zealand

Platz T, Cronin SJ, Cashman KV et al (2007) Transitions from effusive to explosive phases in andesite eruptions—a case-study from the AD 1655 eruption of Mt. Taranaki, New Zealand. J Volcanol Geoth Res 161:15–34

Platz T, Cronin SJ, Procter JN et al (2012) Non-explosive dome-forming eruptions at Mt. Taranaki, New Zealand. Geomorphology 136:15–30

Price RC, McCulloch MT, Smith IEM, Stewart RB (1992) Pb-Nd-Sr isotopic compositions and trace element characteristics of young volcanic rocks from Egmont Volcano and comparisons with basalts and andesites from the Taupo Volcanic Zone, New Zealand. Geochim Cosmochim Acta 56:941–953

Price RC, Gamble JA, Smith IEM et al (2005) An integrated model for the temporal evolution of andesites and rhyolites and crustal development in New Zealand's North Island. J Volcanol Geoth Res 140(1–3):1–24

Procter JN, Cronin SJ, Platz T et al (2010) Mapping block-and-ash flow hazards based on Titan 2D simulations: a case study from Mt. Taranaki, NZ. Nat Hazards 53:483–501

Rowland SK, Jurado-Chichay Z, Ernst G, Walker GPL (2009) Pyroclastic deposits and lava flows from the 1759–1774 eruption of El Jorullo, Mexico: aspects of 'violent Strombolian' activity and comparison with Parıcutin. In: Thordarson T et al. (eds) Studies in Volcanology: The Legacy of George Walker. Geol Soc, Special Publications of IAVCEI, 2:105–128

Salvador A (ed) (1994) International stratigraphic guide. A guide to stratigraphic classification, terminology and procedure, 2nd ed. Subcommission of Stratigraphic Classification of IUGS International Commission on Stratigraphy and Geological Society of America. Boulder, Colorado, 214 pp

Saucedo R, Macías JL, Gavilanes JC, Arce JL et al (2010) Eyewitness, stratigraphy, chemistry, and eruptive dynamics of the 1913 Plinian eruption of Volcán de Colima, México. J Volcanol Geoth Res 191: 149–166

Shane P (2005) Towards a comprehensive distal andesitic tephrostratigraphic framework for New Zealand based on eruptions from Egmont volcano. J Quaternary Sc 20:45–57

Stewart RB, Price RC, Smith IEM (1996) Evolution of high-K arc magma, Egmont volcano, Taranaki, New Zealand: evidence from mineral chemistry. J Volcanol Geoth Res 74:275–295

Stuiver M, Polach HA (1977) Discussion: reporting of 14C data. Radiocarbon 19:355–363

Surono JP, Pallister J et al (2012) The 2010 explosive eruption of Java's Merapi volcano—a '100-year' event. J Volcanol Geoth Res 241-242:121–135

Topping WW (1971) Burrell lapilli eruptives, Mount Egmont, New Zealand. NZ J Geol Geoph 15:476–490

Turner MB (2008) Eruption cycles and magmatic processes at a reawakening volcano, Taranaki. Dissertation, Massey University, Palmerston North, New Zealand, New Zealand

Turner MB, Cronin SJ, Bebbington MS, Platz T (2008a) Developing probabilistic eruption forecasts for dormant volcanoes: a case study from Mt Taranaki, New Zealand. Bull Volcanol 70:507–515

Turner MB, Cronin SJ, Smith IEM et al (2008b) Eruption episodes and magma recharge events in andesitic systems, Mt Taranaki, New Zealand. J Volcanol Geoth Res 177:1063–1076

Turner MB, Bebbington MS, Cronin SJ, Stewart RB (2009) Merging eruption datasets: building an integrated Holocene eruptive record for Mt. Taranaki, New Zealand. Bull Volcanol 71:903–918

Turner MB, Cronin SJ, Bebbington MS et al (2011a) Integrating records of explosive and effusive activity from proximal and distal sequences: Mt. Taranaki, New Zealand. Quaternary Intl 246:364–373

Turner MB, Cronin SJ, Bebbington MS et al (2011b) Relating magma composition to eruption variability at andesitic volcanoes: a case study from Mount Taranaki, New Zealand. GSA Bull 123(9/10): 2005–2015

White JDL, Houghton BF (2006) Primary volcaniclastic rocks. Geology 34:677–680

Whitehead SJ (1976) Granulometric studies on selected tephra eruptions, North Island. Dissertation, Massey University, Palmerston North, New Zealand, New Zealand

Wilson CJN, Houghton BF, McWilliams MO et al (1995) Volcanic and structural evolution of Taupo volcanic zone, New Zealand: a review. J Volcanol Geoth Res 68:1–28

Wilson TM, Stewart C, Sword-Daniels V et al (2011) Volcanic ash impacts on critical infrastructure. J Phys Chem Earth. doi:10.1016/j.pce.2011.06.006

Zernack AV, Procter JN, Cronin SJ (2009) Sedimentary signatures of cyclic growth and destruction of stratovolcanoes: a case study from Taranaki, NZ. Sed Geol 220:288–305

Zernack AV, Cronin SJ, Neall VE, Procter JN (2011) A medial to distal volcaniclastic record of an andesite stratovolcano: detailed stratigraphy of the ring-plain succession of South-West Taranaki, New Zealand. Intl J Earth Scs 100:1936–1966